REPORT DOCUMENTATION PAGE

Form Approved
OMB NO. 0704-0188

1. AGENCY USE ONLY (Leave Blank)	2. REPORT DATE	3. REPORT TYPE AND DATES COVERED
	23 July 2001	Final, 1 Apr. 96 - 31 Mar. 01

4. TITLE AND SUBTITLE
Studies of radar-rainfall error propagation through runoff predictions.

5. FUNDING NUMBERS
G-DAAH04-96-1-0026

6. AUTHOR(S)
Fred L. Ogden, Ph.D., P.E., Principal Investigator
Hatim O. Sharif, Ph.D. candidate

7. PERFORMING ORGANIZATION NAME(S) AND ADDRESS(ES)
University of Connecticut Office for Sponsored Programs
438 Whitney Road Ext., Storrs, CT 06269-4133

8. PERFORMING ORGANIZATION REPORT NUMBER

9. SPONSORING / MONITORING AGENCY NAME(S) AND ADDRESS(ES)
U. S. Army Research Office
P.O. Box 12211
Research Triangle Park, NC 27709-2211

10. SPONSORING / MONITORING AGENCY REPORT NUMBER
~~P-34855-GS-YIP~~
34855.5-EV-YIP

11. SUPPLEMENTARY NOTES
The views, opinions and/or findings contained in this report are those of the author(s) and should not be construed as an official Department of the Army position, policy or decision, unless so designated by other documentation.

12 a. DISTRIBUTION / AVAILABILITY STATEMENT
Approved for public release; distribution unlimited.

12 b. DISTRIBUTION CODE

13. ABSTRACT (Maximum 200 words)
This final report documents the results obtained through the final phase of the research study. It consists of two papers that have been submitted for publication based on the research. THe objective of this project is to quantitatively evaluate the worth of radar-rainfall estimates for physically-based hydrologic modeling. These two papers contain valuable results. To summarize, our study has shown that the physical relationship between radar reflectivity and rainfall rate begins to disappear at a range of approximately 60 km from the radar site for radars with approximately 1 degree beam width. At farther ranges, radar returns are significantly affected by the horizontal and vertical gradients of cloud water. This result was verified through careful testing using a simulation methodology wherein convective rainfall is simulated using the Advanced Regional Prediction Model (ARPS), a radar simulator, and the two-dimensional hydrologic model CASC2D. Techniques to correct runoff predictions for likely errors using a Bayesian approach are suggested.

14. SUBJECT TERMS	15. NUMBER OF PAGES
	108
	16. PRICE CODE

17. SECURITY CLASSIFICATION OR REPORT	18. SECURITY CLASSIFICATION ON THIS PAGE	19. SECURITY CLASSIFICATION OF ABSTRACT	20. LIMITATION OF ABSTRACT
UNCLASSIFIED	UNCLASSIFIED	UNCLASSIFIED	UL

NSN 7540-01-280-5500

Standard Form 298 (Rev.2-89)
Prescribed by ANSI Std. 239-18
298-102

Enclosure 1

PROPAGATION OF RADAR-RAINFALL UNCERTAINTY IN RUNOFF PREDICTIONS

Hatim Osman Sharif, Ph. D.

University of Connecticut, 2001

The primary advantage of radar observations of precipitation compared with traditional rain gauge measurements is their high spatial and temporal resolution and large areal coverage. Unfortunately, radar data require vigorous quality control before being converted into precipitation products that can be used as input to hydrologic models. In this study, a physically-based atmospheric model of convective rainfall is coupled with an active microwave radiative transfer model to simulate radar observation of thunderstorms. Radar observations of these storms are generated and used to evaluate the propagation of radar-rainfall errors through distributed hydrologic simulations. This physically-based methodology allows one to directly examine the impact of radar-rainfall estimation errors on land-surface hydrologic predictions and to avoid the limitations imposed by the use of rain gauge data. Results indicate that the geometry of the radar beam and coordinate transformations, due to radar-watershed-storm orientation, have an effect on radar-rainfall estimation and runoff prediction errors. In addition to uncertainty in the radar reflectivity vs. rainfall intensity relationship, there are significant range-dependent and orientation-related radar-rainfall estimation errors that should be

quantified in terms of their impact on runoff predictions. Rigorous statistical analysis of the relationship between estimated rainfall errors and characteristics of the predicted hydrograph is conducted for thousands of simulated events. In addition to the influence of radar estimation error, the relationship between event magnitude and the prediction error and its propagation is studied. Furthermore, Bayesian inference is applied for estimating the hydrologic output driven by radar-estimated rainfall based on statistical analysis of radar-rainfall error propagation.

TABLE OF CONTENTS

LIST OF FIGURES

LIST OF TABLES

1 INTRODUCTION

Beginning in 1992, the U.S. National Weather Service began upgrading the National Weather Radar network to improve meteorological and hydrologic forecasting. The system of Weather Surveillance Radar-1988 Doppler (WSR-88D) radars was expected to provide high-quality, high resolution precipitation data for the United States that meet a wide range of hydrometeorological applications (*Smith et al.*, 1996). The WSR-88D network consists of about 140 radar systems providing nearly continuous coverage of the United States (*Crum and Alberty*, 1993). The system collects, processes, and displays high-resolution reflectivity, mean radial velocity, and spectral width data. One of the primary purposes of the system is to provide real-time detection of severe weather phenomena including tornadoes, mesocyclones, and downbursts. Another important use of the system is to provide accurate predictions of extreme rainfall leading to flash floods and rainfall over large river basins used by National Weather Service River Forecast Centers.

The primary advantage of radar rain products is their high spatial and temporal resolution and large areal coverage. Severe flood and flash flood forecasting (*Georgakakos*, 1986a,b) and urban storm runoff modeling (*Ogden et al.*, 2000) require high resolution precipitation data. Other applications such as water resources planning and management (*Flach et al.*, 1991) and long-term water supply forecasting at time scales of weeks to months and spatial scales ranging over many orders of magnitudes (*Smith et al.*, 1992) require accurate information on the total precipitation amounts over large spatial domains.

One of the main factors affecting the accuracy of physically-based hydrologic simulations is rainfall input uncertainty. Rain gages suffer from undercatchment and a number of spatial and temporal sampling deficiencies. Although ground-based weather radars provide rainfall rate estimates over large areas at high spatial and temporal resolutions, radar data require vigorous quality control before being transformed into precipitation products that can be used as input to hydrologic models. The relationship between radar reflectivity and surface rainfall is highly complex (*Austin*, 1987). In addition to the difficulties in estimating the parameters of the equation that relate the reflectivity to the rainfall intensity, there are many other physical factors that increase the uncertainty of radar-rainfall estimation. The impact of radar-rainfall estimation errors on hydrologic predictions from physics-based models is an important area of study, with broad implications ranging from study of global climate change to watershed ecology and engineering hydrology.

The main objective of this research is to develop a comprehensive methodology to investigate the propagation of radar-rainfall errors through Hortonian runoff predictions. The research consists of two parts:

1) Numerical Simulation of Radar-Rainfall Error Propagation: In this part, a simulation methodology is developed to examine the propagation of radar-rainfall estimation errors, due to a variety of causes, through Hortonian runoff predictions. An atmospheric model is used to generate convective storms and an active microwave radiative transfer model

is used to simulate the propagation of electromagnetic waves between the radar and the storms. Radar-estimated rainfall from simulated storms serve as input to a calibrated (for a certain actual basin), physically-based, infiltration-excess, watershed model to study the propagation of radar-rainfall estimation errors. In addition to the influence of radar range and radar orientation, systematic and random errors are imposed on the radar estimation process to study their impact on runoff prediction.

2) Statistical Analysis of Radar-Rainfall Error Propagation: In this part, a storm that covers a large area is simulated and the location of the study watershed is moved within the storm domain to obtain different realizations of the storm over the watershed. The rainfall field generated by the atmospheric model is assumed to be the ground "truth". The radar simulator is then run and radar-estimated rainfall from the simulated storm is used as input to a calibrated (for a certain actual basin), physically-based, infiltration-excess, watershed model to analyze the propagation of radar-rainfall estimation errors. The spatial and temporal structures of the precipitation field, combined with the use of 500 hundred locations within the storm domain, help develop a large set of rainfall events with different rainfall volumes and vertical reflectivity profiles and analyze statistics of the "true" and estimated hydrologic outputs. In addition to the influence of radar range and radar orientation, the relationship between the rainfall event magnitude and the prediction error is studied. Furthermore, Bayesian inference is applied for estimating the hydrologic output driven by radar-estimated rainfall based on statistical analysis of radar-rainfall error propagation.

2 NUMERICAL SIMULATIONS OF RADAR-RAINFALL ERROR PROPAGATION

ABSTRACT

The primary advantage of radar observations of precipitation compared with traditional rain gauge measurements is their high spatial and temporal resolution and large areal coverage. Unfortunately, radar data require vigorous quality control before being converted into precipitation products that can be used as input to hydrologic models. In this study, we coupled a physically-based atmospheric model of convective rainfall with an active microwave radiative transfer model to simulate radar observation of thunderstorms. We used the atmospheric model to simulate a well-documented tornadic supercell storm that occurred near Del City, Oklahoma on May 20, 1977. We then generated radar observations of that storm and used them to evaluate the propagation of radar-rainfall errors through distributed hydrologic simulations. This physically-based methodology allows us to directly examine the impact of radar-rainfall estimation errors on land-surface hydrologic predictions and to avoid the limitations imposed by the use of rain gauge data. Results indicate that the geometry of the radar beam and coordinate transformations, due to radar-watershed-storm orientation, have an effect on radar-rainfall estimation and runoff prediction errors. In addition to uncertainty in the radar reflectivity vs. rainfall intensity relationship, there are significant range-dependent and orientation-related radar-rainfall estimation errors that should be quantified in terms of their impact on runoff predictions. Our methodology provides a tool for performing experiments that address some operational issues related to the process of

radar-rainfall estimation and its uses in hydrologic prediction.

2.1 Introduction

The performance of distributed, physically-based hydrologic models depends greatly on the quality of the input data. The most important input is rainfall because such models are very sensitive to it [*Julien and Moglen*, 1990], particularly models of Hortonian [*Horton*, 1933] runoff. Errors in the space-time description of rainfall are often amplified through Hortonian runoff predictions [*Ogden and Sharif*, 2000]. The shortcomings of rain gauge networks are well documented. Rain gauges do not represent areal rainfall at the watershed scale well because they are merely point samples, while watersheds are more sensitive to the spatial distribution of rainfall. The use of rain gauge data necessitates spatial interpolation of the rainfall data. The accuracy of the resultant rainfall fields is limited by the correlation structure of rainfall and the network density.

The primary advantage of radar precipitation products is their high spatial and temporal resolution and large areal coverage. Severe flood and flash flood forecasting [*Georgakakos*, 1986a,b] and urban storm runoff modeling [*Ogden et al.*, 2000] require high-resolution precipitation data. Early assessments of the usefulness of radar-rainfall estimation errors in flow forecasts [e.g. *Barge et al.*, 1979] were optimistic. However, more recent studies have shown that the impact of radar-rainfall estimation errors on runoff predictions can be very significant in certain situations.

The National Weather Service (NWS) has updated its weather radar capabilities with the deployment of over 120 WSR-88D (Weather Surveillance Radar, 1988-Doppler) radars. The WSR-88D radar network provides the 48 contiguous United States with nearly continuous radar coverage below 3000 m above sea level, except where rising terrain occludes low elevation angle scans. The WSR-88D system represents a significant advance in the field of operational hydrology over older technology. The system provides a large number of diverse hydrometeorological products [*Fulton et al.*, 1998].

Unfortunately, there are no unique relationships between the radar-measured reflectivity and the rainfall rate. The relationship between radar reflectivity and surface rainfall is highly complex [*Austin*, 1987]. In addition to the difficulties in estimating the parameters of this relationship, there are many other physical factors that increase the uncertainty of radar-rainfall estimation. Radar-rainfall estimates are always at risk of being contaminated by a host of random and systematic error sources. Some of the other potential sources of errors are: radar hardware calibration, the deflection of the radar beam from its path (Anomalous Propagation), the attenuation of the electromagnetic wave by rain and atmospheric gases, the presence of frozen hydrometeors and the melting layer, and range effects. A discussion of numerous sources of radar-rainfall estimation error is also found in *Wilson and Brandes* [1979], *Zawadzki* [1982, 1984], *Krajewski and Smith* [1991].

The need to improve hydrologic predictions indicates the increased importance of

research efforts in the dynamic numerical modeling of quantitative precipitation, either through explicit treatment or through parameterization. The dynamic (physically-based) models of rainfall are usually based on sets of partial differential equations, which describe conservation of mass, momentum, and energy in the atmosphere. Subgrid-scale physics are parameterized using grid scale variables. These equations are integrated numerically in time in a 3-dimensional model domain to produce predictions of rainfall, in addition to a complete set of state variables. The past two decades have seen increased usage of explicit cloud models in the simulation and prediction of convective storms [e.g., *Klemp et al,*. 1981; *Droegemeier et al.*, 1996; *Xue et al.*, 1996a; *Xue et al.*, 1996b]. Significant progress has been made in the use of radar observations to initialize real storms and produce realistic forecasts of intense precipitation systems [e.g., *Lin et al.*, 1993; *Shapiro et al.*, 1996; *Gao et al.*, 1998; *Sun and Crook*, 1998; *Grecu and Krajewski*, 2000a,b]. Numerical, physically-based modeling of storms facilitates our understanding of the three-dimensional variability of hydrometeor characteristics. When modeled storms are coupled with a scheme for simulating the physics of electromagnetic wave propagation, the simulation system provides an opportunity to study some aspects of the complex relationship between radar observables and the true (although simulated) rainfall fields and the impacts of radar-rainfall estimation errors on runoff predictions.

2.2 Objectives

In this paper, we use a simulation methodology to examine the propagation of radar-rainfall estimation errors, due to a variety of causes, through Hortonian runoff predictions. We use an atmospheric model to generate convective storms and an active microwave radiative transfer model to simulate the propagation of electromagnetic waves between the radar and the storms. This methodology allows us to assume that the rainfall fields generated by the atmospheric model are the "truth". We use radar-estimated rainfall from simulated storms as input to a calibrated (for a certain actual basin), physically-based, infiltration-excess, watershed model to study the propagation of radar-rainfall estimation errors. In addition to the influence of radar range and radar orientation, we impose systematic and random errors on the radar estimation process to study their impact on runoff prediction. Our simulation methodology allows us to avoid the traditional approach of assessing radar estimates accuracy by comparisons with rain gauges, which is subject to several fundamental limitations [*Zawadzki,* 1975*; Ciach and Krajewski,* 2000]. Furthermore, we simulate the radar estimation process below the freezing level to avoid the complex ice microphysics and "bright band" effects. We also analyze the effect of adjusting radar-rainfall estimates on predicted runoff.

2.3 The Tools

2.3.1 The Atmospheric Model

The Advanced Regional Prediction System (ARPS) is a general purpose, nonhydrostatic, compressible model for storm- and meso-scale atmospheric simulation and

real-time numerical weather prediction [*Xue et al.*, 1995; *Xue et al.*, 2000a; *Xue et al.*, 2000b]. The model was developed at the Center for Analysis and Prediction of Storms (CAPS) at the University of Oklahoma, with the support of the National Science Foundation Science and Technology Center (STC) program. The model solves equations for momentum, temperature, pressure, water substances, and subgrid-scale turbulent kinetic energy, and includes comprehensive physical processes. The model serves as an effective tool for both basic research and for operational numerical weather prediction [e.g., *Droegemeier et al.*, 1996; *Xue et al.*, 1996b]. Additional examples of the model applications can be found in *Xue et al.*, [2000a,b].

2.3.2 The Radar Simulator

Krajewski et al., [1993] proposed a physically-based simulation of radar observations based on a two-dimensional stochastic space-time model of rainfall events and a statistically generated drop-size distribution. *Anagnostou and Krajewski* [1997] made several extensions to this simulator. The two-dimensional fields were complemented with a vertical structure of hydrometeors by choosing a cloud type model, which resulted in size, shape, and phase (mixed or single) distribution at discrete elevations. Recently, *Anagnostou et al.* [2000] used the simulator in their study of NEXRAD radar calibration based on a comparison with the TRMM satellite [*Kummerow et al.*, 1999].

We modify the radar simulator in this study to calculate various radar observables

from the three-dimensional output produced by the ARPS atmospheric model. We modify the beam geometry to capture the high variability within convective systems. The simulator extracts three-dimensional estimates of pressure, temperature, cloud rainwater content, and water vapor content from ARPS, and uses these outputs to calculate the mixing ratios of rainwater and the gradients of the atmospheric refractive index. We simulate beam propagation in a three-dimensional space. The simulated radar measurement process includes integrating over the pulse volume using a Gaussian beam power distribution. We use the default WSR-88D Z-R relationship of $Z=300R^{1.4}$ [*Fulton et al.*, 1998], to convert reflectivities into rainfall rate estimates. The radar wavelength is assumed to be 10 cm, the beam elevation angle is 0.5°, and the half-power beam width is 1°, close to WSR-88D's value of .95°. The azimuthal resolution of radar observations is 1°.

2.3.3 The Hydrologic Model

The hydrologic model used in this study is the physically-based, distributed parameter, Hortonian, finite difference model CASC2D (CASCade of planes, two-dimensional) [*Julien et al.*, 1995; *Ogden,* 1998]. The model accepts fully spatially-varied rainfall input, uses *Green* and *Ampt* [1911] infiltration with redistribution [*Ogden and Saghafian*, 1997], two-dimensional diffusive-wave overland flow routing, and one-dimensional diffusive-wave channel routing. CASC2D has the capability to model a variety of channel cross-sections (*Ogden*, 1994), and includes continuous soil moisture accounting [*Ogden and Senarath*, 1997; *Senarath et al.*, 2000]. The model was also used in a flash flood simulation study in

which perennial and ephemeral lakes were modeled [*Ogden et al.*, 2000]. The model uses a square grid representation of the watershed at a user-selected grid size. Once ponding occurs, surface water is accumulated in each model grid cell until the specified retention depth for that cell is exceeded. Thereafter, the overland flow is routed into two orthogonal directions. When overland flow reaches a model grid cell that contains a defined channel, the flow is passed into the channel and routed using a one-dimensional explicit diffusive-wave routine.

2.4 The Study Watershed

The watershed used in this study for hydrologic simulations is the 21.2 km^2 Goodwin Creek experimental watershed located in north-central Mississippi. The USDA-ARS National Sedimentation Laboratory has continuously monitored the watershed since 1981. *Alonso* [1996] provides a detailed description of the watershed. The elevation of the watershed ranges from 68 to 127 m. The main channel has an average slope of 0.004 [*Bingner*, 1996]. The grid size used in CASC2D to model the watershed is 125 m ×125 m, to minimize computing time yet adequately describe the spatial variability of topography, soil texture, and land use/land cover. Hortonian runoff is dominant and the contribution of groundwater to runoff is insignificant in the watershed. The groundwater table is several meters below surface; according to measurements, it varies by only 5-10 cm near channels during significant runoff events. The base flow at the outlet of the catchment is typically below 0.05 m^3/s. The

hydrologic model CASC2D was rigorously calibrated on this watershed by *Senarath et al.*, [2000] and thus we feel the model represents the watershed's runoff processes with reasonable accuracy.

2.5 Numerical Framework

2.5.1 ARPS Simulations

Within the framework of this methodology, we simulate a well-documented tornadic supercell storm that occurred near Del City, Oklahoma on May 20, 1977, using the ARPS. This storm has been studied extensively using both multiple Doppler radar analysis and numerical simulation. For details on storm morphology and evolution, the readers are referred to *Ray et al.*, [1981] and *Klemp et al.*, [1981].

We simulate two hours of the storm's total duration. The simulation starts from a thermal bubble placed in a horizontally homogeneous base state, specified from the sounding used in *Klemp et al.*, [1981]. Like *Klemp et al.* [1981], we subtract a mean storm speed (U=3 ms^{-1}, V=14 ms^{-1}) from the sounding, to keep the right-moving storm near the center of the model domain.

The model grid consists of 67×67×35 grid points with a uniform grid interval of 1 km in the horizontal and 0.5 km in the vertical direction. The physical domain size is therefore

$64\times64\times16$ km^3. The initial bubble was centered at x=48 km, y=16 km and z=1.5 km and has a maximum perturbation of 4 °K. The radius of the bubble is 10 km in both the x and y directions and 1.5 km in the vertical. We use the *Kessler* [1969] warm rain microphysics option together with a 1.5-order turbulent kinetic energy sub-grid turbulence parameterization. We also use open boundary conditions at the lateral boundaries and an upper-level Rayleigh damping layer.

Between 30 and 60 minutes, the simulated storm underwent a splitting process (Figs. 1a and 1b), with the right-moving (relative to the environmental wind shear vector, which points in the northeast direction) cell remaining near the center of the domain, and the left-moving cell propagating to the northwest corner of the domain. The precipitation rates from the simulated storm at 30 minute intervals are shown in Figure 1 (only 3/4 of the simulation domain in terms of the length of each side is shown), corresponding to 30, 60, 90, and 120 minutes after initiation of the storm. The use of a moving coordinate system (through the deduction of a mean wind) makes the simulated storm, especially the right-moving cell, appear roughly stationary relative to the grid. Relative to the ground, the storm moves at speeds ranging from approximately 3 to 14 m/s.

The patterns of the surface precipitation rate usually resemble the pattern of radar reflectivity fields. The hook-shaped pattern associated with the right moving cell is also associated with the so-called hook echoes that demonstrate the strong rotation associated

with tornadic supercell thunderstorms. In this simulation, the left-moving cell is actually stronger (Fig.1c). The evolution of the simulated storm is qualitatively similar to the observed storm [*Ray et al., 1981*], and after two hours, it has attained a structure typical of mature supercell storms.

We show a sample of vertical reflectivity profiles that we compute using the storm hydrometeor fields in Figure 2. The solid line represents the mean reflectivity profile. The reflectivity profiles, including the mean, are similar to the profiles reported in the literature [e.g. *Szoke et al.*, 1986a,b] and the profiles from the WSR-88D data [*Vignal and Krajewski*, 2000]. The spatial correlation within the storm, and the fractional areal coverage of the storm based on rainfall intensity, also shown in Figure 2, are similar to some of those found in the literature (e.g. *Calheiros*, 1984). This similarity also indicates that ARPS output is reasonably representation of a convective storm.

2.5.2 Radar-Storm-Watershed Orientation

Since radar beams rise and widen with range, the radar-viewing aspect of a storm may have an effect on the radar estimates for a highly variable three-dimensional convective cell. Different orientations result in different coordinate geometry, and volumetric averaging of radar observables. To investigate these effects quantitatively, we place our virtual radar at 24 equi-spaced orientations (every 15°). We also vary the range along these directions as illustrated in Figure 3. Since the storm domain is significantly larger than the study

watershed, we vary the watershed location within the storm. Because of the high variability within the convective storm, we move the watershed to ten different locations within the storm domain to obtain different cases of the radar estimation process. The ten locations do not overlap and are sufficiently far apart from each other to be considered independent storm realizations.

We assume the hydrographs simulated using CASC2D, driven by the "true" ARPS rainfall fields, are the "true" runoff hydrographs. We use four measures for comparing these "true"-rainfall-based simulations with the ones based on radar-estimates: the watershed total rainfall volume ratio, the root mean square error in the simulated hydrograph, the total runoff volume ratio, and the peak discharge ratio.

In addition to the effects of range and orientation, we also studied the effects of both systematic and random errors. Random errors resulting from the uncertainty in the relationship between the radar reflectivity and the rainwater mixing ratio, or radar system noise, and additive calibration drifts, were imposed to study their impact. The simulator computes radar observables using either a constant value for the slope of the refractive index or a value calculated from atmospheric variables to study the impact on the hydrologic model output. We compute the attenuation of electromagnetic waves by rain as a function of the radar wavelength (10 cm), rainfall intensity, and the distance between the radar and the hydrometeors. The attenuation from atmospheric gases, which is typically larger than rain

attenuation for S band, is only a function of radar wavelength and distance [*Doviak and Zrnic*, 1993]. We do not model atmospheric gases attenuation because this effect is taken care of in real radar data processing systems.

Finally, we multiply radar-rainfall estimates by a factor that makes the watershed total rainfall volume equal to the "true" rainfall volume, for all ranges and orientations, and compare the resulting outputs of the hydrologic model to the "true" hydrologic outputs. This is done to assess the quality of the hydrologic outputs driven by adjusted radar-rainfall estimates.

2.6 The Results

2.6.1 Simulations With No Imposed Errors

In the first part of this study, we assume that the simulated radar measurement process is error-free to study the pure effects of range and orientation between the radar and study watershed. The closest radar position we test is 10 km from the center of the watershed. We then gradually increase the range at an increment of 5 km, up to 145 km from the center of the watershed. We limit the range to 145 km in order to avoid the influence of the freezing level on the radar-measured reflectivity for the storm being studied.

To quantify the effects of radar orientation, we place the radar at 24 equi-spaced orientations (every 15°), and vary the range in these directions, as illustrated in Figure 3. The 28 range increments are the same for all 24 radar orientations. The orientations are coded

with numbers 1 through 24, orientation 1 being exactly east of the watershed center. We distribute the orientations over 360° because of the asymmetry of the simulated storm. Radar rainfall estimates are entered into the hydrologic model in polar coordinates, and we apply the nearest neighbor method to interpolate rainfall rates for each hydrologic model grid.

The rainfall volume error measure is the ratio between the radar-estimated catchment total rainfall volume and the "true" total rainfall volume predicted at the ground level by the atmospheric model. The measurements of the influence of radar error on hydrologic model response are three of the statistics that are typically used to calibrate hydrologic models and evaluate their performance [e.g. *Brazil*, 1988; *Senarath et al.*, 2000]. Root mean square error (RMSE) is computed from:

$$RMSE = \sqrt{\frac{1}{N}\sum_{i=1}^{N}(q_i^{est} - q_i^{ref})^2} \qquad (1)$$

where q^{est} is the simulated discharge driven by radar-estimated rainfall and q^{ref} is the corresponding discharge resulting from the reference ARPS modeled rainfall (i.e., we assume the hydrograph produced using ARPS rainfall fields to be the reference hydrograph). N refers to the total number of hydrograph ordinates used in the analysis, while i is the index denoting individual hydrograph ordinates. RMSE is expressed as a percentage of the reference peak discharge.

The error in peak discharge is expressed as the ratio between the estimated peak

discharge and the "true" peak discharge. The error in runoff volume is similarly expressed as the ratio of the estimated and reference total runoff volumes.

2.6.2 Effects Of Range/Orientation

We show the combined effects of range and orientation on the estimated rainfall field in Figure 4a. These are the results from a set of simulations with the watershed at one of the ten locations tested within the storm domain. Each curve in the graph represents one of the radar orientations. The effect of range is clear on all 24 lines, and the scatter resulting from orientation effect is significant. The scatter is very small at the 10 km range, and increases steadily with range. The largest scatter occurs when the radar is 145 km from the center of the watershed, the farthest range we tested. The scatter varies from 2% to about 17% of the total rainfall volume. In all the plots of Figure 4, curves adjacent to each other generally represent orientations that are close together, for example, in Figure 4a, the line representing orientation 7 is adjacent to the line representing orientation 6. Lines representing orientations 180 degrees apart are generally adjacent to each other for small ranges and start to diverge with increasing range. Most of the 24 lines follow a distinct pattern, which is a gradual decrease with increasing range to about 100-110 km, followed by a more rapid increase with increasing range. This is clear in Figure 5a, which shows the mean for the 24 orientations. The maximum average rainfall volume error is 24% at a range of about 100 km. The standard deviation of the 24 rainfall volume ratios increases almost linearly with range, as seen in Figure 5a. The response to the combined effect of range and orientation is similar for the

other nine watershed locations.

The error in the predicted runoff is somewhat different. Radar-rainfall estimation errors are generally amplified through predicted runoff. The variance in predicted runoff volume is more than double that for the rainfall volume, as shown in Figure 4b. The average value of runoff volume error, shown in Figure 5b, whether from underestimation or overestimation, is twice the average rainfall volume error (Figure 5a) even though the curves in both graphs follow a similar trend. The standard deviation of the 24 runoff volume ratios, shown in Figure 5b, is about twice that of rainfall volume ratios, and the increase with range is similar to that of the rainfall volume curve. The runoff simulations show that both range and orientation errors are amplified in the predicted runoff. The graphs representing the error in peak discharge (Figure 4c) are similar to runoff volume error graphs. Interestingly, for some orientations there is no significant change in the peak discharge error after the range of 100-110 km (Figure 4c), which suggests that rainfall volume errors are compensated for by other errors. The graph of the hydrograph root mean squared error (RMSE), shown in Figure 4d, has a linear-convex-concave shape. The linear portion corresponds to the region where the rainfall (or runoff) is overestimated. This part shows a small change with range. The convex portion of the curve corresponds to the region where overestimation decreases and underestimation starts. The curve becomes concave as the underestimation continues with range, and the slope changes sign as the underestimation begins to decrease. The scatter due to orientation increases with range, but the general pattern is different from other graphs,

because the RMSE graph shows whether there is underestimation or overestimation.

We summarize rainfall and runoff statistics from ARPS simulations for the ten watershed locations in Table 1 and the average values of error statistics in Figure 6. The mean rainfall volume error curves (Figure 6a) show a different trend, due to the fact that each location represents an independent realization of the storm. The curve showing the highest error corresponds to the watershed location with the smallest total rainfall accumulation (Location 6 in Table 1). The watershed response depends largely on the rainfall error, and also on the magnitude of the rainfall volume, and the spatial distribution of the rainfall (Figures 6b and 6c). The increase of RMSE with range is drastic for the location with the smallest rainfall accumulation (Figure 6d). For two locations, RMSE decreases with range. At these two locations, with some of the highest rainfall accumulations, the estimated rainfall volume on the watershed is smaller than the "true" rainfall volume and it increases slightly with range. Nevertheless, the scatter due to orientation increases with range for these two locations as well.

2.6.3 Effect Of Imposed Errors

To study the effects of random and systematic radar measurement errors when combined with orientation and range effects, we impose noise on reflectivities measured by the radar simulator. It is a well-established fact from disdrometer studies, that there is no unique relationship between rainwater mixing ratio (M) and radar reflectivity (Z). *Steiner and*

Smith, [2000] conducted an exhaustive study of two-years-worth of disdrometer data at the Goodwin Creek, where they reported larger anomalies in the Z-R relationship. They found that the uncertainty in Z-R relationship due to 1-minute raindrop spectra variability was approximately 40%-50% as characterized by root-mean-square-error. Increasing the time averaging from 1 minute to 5 minutes had little effect on the raindrop spectra variability. We add a normally distributed random error, N(0,1) (i.e., with a mean of 0 and a standard deviation of 1 dBZ), to the radar reflectivity estimates, which are based on a unique relationship between Z and M, to account for the randomness in Z-M relationship. The ±3 dBZ range of this error agrees with the values reported in several studies [e.g., *Steiner and Smith,* 2000]. This N(0,1) noise can also account for random noise in radar system measurement, such as from a transmitter, receiver, antenna, wave guide, or signal processing error, that corrupts the measurement process.

The radar equation relates radar-measured power to characteristics of the radar and characteristics of the precipitation targets [*Doviak and Zrnic*, 1993;. *Smith et al.,* 1996] argue that radar calibration, which is dependent on the value of the constant of the radar equation, plays an important role in site-to-site differences in WSR-88D precipitation estimates. *Hunter*, [1996] reports that drifts in absolute radar calibration cause differences of more than 17% at the same location from adjacent WSR-88D's. We evaluate the effect of radar calibration errors (drifts) in two additional simulations: a calibration error (drift) of 2 dBZ is added to radar reflectivity measurements in one simulation, and subtracted in another.

We select these systematic and random errors as examples of the many errors associated with the radar measurement process to determine their impact on hydrologic predictions.

We show the impact of the imposed errors on estimated predicted rainfall volume error and hydrograph RMSE in Figures 7a through 7d. These results are for two different orientations at the same location that we presented in Figure 4. Random noise from the M-Z relationship, or radar system measurement noise, has a small impact on error statistics; it generally decreases the smoothness of individual lines.

The impact of the calibration error alone on the estimated rainfall can be easily quantified by adding the amount of drift (dBZ) to the measured Z value. The effect is different when combined with range/orientation. Calibration error effects can either amplify or reduce range/orientation error. This is especially clear in hydrograph RMSE curves. In some cases, estimates of rainfall volume with imposed calibration errors are better than error-free estimates at far ranges. This is a clear example of the difficult task of trying to isolate separate radar error sources. Radar calibration errors have large effects on all three simulated runoff error statistics.

2.6.4 Effect Of Non-Uniform Refractive Index

In all simulated runs, the gradient of refractive index has a constant value of -.0000393. In one simulation run we calculated the gradient of the refractive index at each

grid of the atmospheric model, using the equation relating the refractive index to atmospheric variables [e.g. *Battan*, 1983]. We then calculated the effect on the path of the propagated radar beam and hence the effect on radar rainfall estimates. When the values of refractive index gradient, which were computed at each atmospheric model grid cell, were used, hydrologic predictions were not significantly affected. In all simulations, the terrain is assumed to be perfectly flat and problems of anomalous propagation are not addressed.

2.6.5 Adjustment Of Radar Estimates

We adjust the radar-estimated rainfall accumulations to match the ARPS rainfall accumulations on a storm-total basis in order to examine hydrologic model performance using the adjusted radar-rainfall fields as input. We multiply radar estimates by a factor such that radar estimated rainfall volumes, for all ranges and orientations, equal the ARPS rainfall volume, as we did for the radar location analyzed in Figure 4. We find that the predicted runoff volume is practically the same as the reference runoff volume, with small scatter, up to a range of about 70 km. The error in predicted runoff volume increases steadily with an increase in the scatter, as shown in Figure 8b, for ranges beyond 70 km. The runoff volume error driven by adjusted radar estimates can reach up to 14% at a 145 km range for some orientations. The error in peak discharge is larger than the error in runoff volume, and the scatter increases appreciably at ranges beyond about 90 km. The maximum error for some simulations is close to 35%, at 125 km. The hydrograph RMSE graph is similar to the peak discharge error graph with a maximum of about 11% of the peak discharge.

Comparing Figure 4 and Figure 8 shows the effect of radar adjustment. Note that in this study we assume that perfect storm total rainfall volume adjustment is possible. In reality, this does not occur. For example, multisensor precipitation estimates [*Krajewski*, 1987; *Seo*, 1998] are obtained by adjusting radar estimates using rain gauge data. Consideration of other error sources associated with real multi-sensor adjustments is beyond the scope of this paper.

2.6.6 ARPS Model Resolution Effects

The atmospheric model grid size, 1.0 km horizontal and 0.5 km vertical, is a factor in determining the values of the computed range/orientation errors, but it is not the main cause of the errors. We investigate this using output from two additional ARPS simulations of the same storm with higher resolution outputs: 0.5 km horizontal and 0.5 km vertical, and 0.25 km horizontal and 0.25 km vertical. Simulations with these finer resolution three-dimensional atmospheric fields showed no reduction in the average radar range/orientation errors. There are minor differences between the results of the two higher resolution simulations, which demonstrate that for this storm there is no practical accuracy gained for resolutions higher than 0.5×0.5×0.5 km.

Rainwater mixing ratios have discrete values at each ARPS grid. To further assess the impact of the discrete nature of the ARPS output, we use simulated radar observations of simple, hypothetical rainfall fields. The variations between rainwater mixing ratios are

assumed to be continuous (not discrete) within the simulated domain, which covers a rectangle of 7 km by 10 km. The vertical profile of rainwater mixing ratios follows a General Extreme Value distribution GEV (1.0,1.0,-0.1), $f_1(z)$, where the X-axis variation follows a Gumbel distribution G(19.0,3.0), $f_2(x)$, and the Y-axis variation follows a Gumbel distribution G(15.0,4.5), $f_3(y)$. At every point, p(x,y,y), the rainwater mixing ratio is calculated by the relationship $M= f_1(z)*f_2(x)*f_3(y)*0.625$ kg/m^3. We admit that these are not realistic rainfall fields, since no real storm can be so smooth. They are only meant to serve as illustrative examples of the measurement errors under consideration. Note that the vertical profile of reflectivity is a function of z only and does not vary horizontally. Radar-rainfall estimates of these simulated fields have range/orientation errors, which increase with range. Errors are also amplified in the predicted runoff. Real storms, like the Del City storm, show significant randomness in horizontal and vertical variability, which also contributes to the range/orientation effects.

A closer look at the geometry of the radar pulse volume, beam propagation path, elevation and azimuthal angle reveals some of the aspects of the range/orientation effects. For two radars at orientations 180° apart, the sampling volume is almost identical when the beams are concentric and the same distance away from the two radars at near ranges, particularly if they are on the line that connects the two radars. Sampling volumes that are on the straight line between the two radars are still very similar at close ranges but the difference increases with increasing range. At points not on this line and at different distances from the two

radars, there can be significant differences in the size, height, and orientation of the sampling volumes, resulting in large differences in radar estimates. This can be illustrated by considering the differences between radar rainfall estimates at orientation 1 and orientation 13, as shown in Figure 3. To ensure that grid size does not cause these discrepancies, we analyze the case of the hypothetical rainfall fields mentioned above. In Figure 9, we show the locations of radar pulse volume centers within the rectangle that encompasses the watershed for the two radars at ranges of 10 km and 145 km. We compute the differences between the radar estimates at each location. At the smallest practical range we are considering, the differences are negligible at the center where the two beams are almost concentric and at equal distance from the two radars. On the line perpendicular to the line connecting the two radars, where the beams are not exactly concentric but approximately at equal distance from the two radars and at the same height, the maximum difference in point estimates of rainfall rate is about 1% on the edges of the rectangle. On the line connecting the two radars, the maximum difference at the edges of the rectangle is 3%. At the corners of the rectangle, it is about 4%. The difference in estimated total rainfall volume is about 1%.

The picture is quite different at the 120 km range. At the center of the watershed, the difference is 3%. This is due to differences in the sampling volume between the two radar beams. The differences on the edges of the perpendicular line are 9%. On the line between the two radars, the maximum difference is 10% and the difference in total estimated rainfall volume on the watershed is 6%. This is an illustration of the range/orientation effect and the

numbers are a sample of these errors. Note that in the above analysis, the vertical profile of the rainwater mixing ratio does not vary horizontally.

The azimuthal resolution is one of the factors that control the orientation effect. In a test run, where we changed the azimuthal resolution from 1° to .3° by oversampling, and the scatter at far ranges was reduced by about 30%. Reducing the radar beam width attains similar reduction in orientation effects.

The choice of the Z-R relationship in this study is arbitrary. Our simulations show that small changes to the Z-R relationship parameters have no significant effects on the hydrologic outputs, e.g., changing the multiplicative coefficient from 300 to 400, and the power coefficient from 1.4 to 1.3, changes the outputs by less than 5%.

2.7 Discussion

The propagation of the radar beam is accompanied by an increase in the radar sampling volume and an increase of the height of the radar beam center, with range depending on elevation angle, earth curvature and gradients of atmospheric refraction index. These two factors cause several errors (e.g., smoothing of reflectivity gradient and overshooting of precipitation) and also play a role in the presence of the orientation effect, which increases with range.

All the simulations in this study highlight the range/orientation effects for convective storms and their propagation through hydrologic model predictions for a 21 km^2 watershed. It is well known that other factors in the radar-rainfall measurement/estimation process can cause errors larger than the errors we discuss here. However, pinpointing and quantifying these errors provide incentive to study these errors and search for means to adjust them. We do not think that these simulations, which demonstrate examples of the impact of high variability within convective cells, present worst case scenarios in small sized watersheds. We have chosen error statistics at the watershed scale (e.g., we did not considered errors in instantaneous values of variables at the pulse volume scale). For larger watersheds, there might be similar range/orientation errors, at least at smaller temporal or spatial scales. For example, *Ogden and Julien*, [1994] found that the effect of radar data resolution depended upon "storm smearing" and "watershed smearing". Storm smearing occurs when the radar rainfall data resolution is coarser than the rainfall spatial correlation length. Storm smearing reduces rainfall gradients and is independent from the watershed size. Watershed smearing occurs when the radar rainfall data resolution exceeds 40% of the square root of the watershed, creating uncertainty with regard to the location of precipitation relative to the watershed boundary. Watershed smearing is the main source of hydrologic model error in very small subcatchments. However, for the 21 km^2 Goodwin Creek watershed used in our study, storm smearing is the dominant error source.

2.8 Summary And Conclusions

We developed a simulation framework for the study of the hydrological impacts of radar-rainfall estimation errors. The simulation framework is physically-based and consists of an atmospheric model, a simulator of radar observations, and a distributed hydrologic model. The storm we used in our study is well-documented and is considered a benchmark storm for the validation of atmospheric models (see ARPS references). The rainfall fields we simulated in this study are adequately realistic and can serve as an example of supercell storms that cause flash flooding in small and mid-sized watersheds. Although we use only single-polarization radar-reflectivity in this study, the radar data simulator has the capability to generate multi-parameter radar observables (e.g., differential reflectivity and differential propagation phase shift). Using our approach, it is possible to simulate several sources of radar measurement and estimation errors, both systematic and random.

The distributed physically-based hydrologic model CASC2D [*Julien et al.*, 1995; *Ogden*, 1998] we use in the study is rigorously calibrated [*Senarath et al.*, 2000] on an extensively-monitored research watershed. This leads us to believe that the propagated errors in predicted runoff provide examples of what to expect in real world hydrologic studies using a physically-based, distributed, Hortonian model.

Range effects are caused primarily by the vertical profile of reflectivity and the size of the radar pulse volume. The differences in radar predictions caused by the orientation

between the radar, the storm, and the watershed (see Figure 4a for an example) mainly depend on the size of the pulse volume and the sampling resolution. Though it is not practically feasible, two identical radars at two different orientations could hypothetically give identical measurement of a storm, if there were no vertical variability and the radar pulse volume and azimuth resolution were small enough to capture the horizontal variability, and if we were to neglect attenuation effects. The actual difference between the two estimates depends on the radar pulse volume, the azimuthal resolution, and the vertical and horizontal variability within the storm, among other factors. Decreasing the azimuthal resolution can remove a large portion of the orientation effects. Measurements by two or more radars of the same storms were discussed in several radar-rainfall estimation studies [e.g. *Smith et al.*, 1996; *Ogden et al.*, 2000] and in studies of radar data assimilation [e.g. *Sun et al.*, 1991; *Sun and Crook*, 1998]. The orientation effects we investigate give rise to many interesting questions: Do the radar estimation/measurement errors cancel each other out? Does the mosaicing of the multiple radar data help reduce errors? Does a miscalibrated radar always give inferior estimates compared to a well calibrated one?

Hydrologic simulations demonstrate that range orientation errors are typically amplified through predicted Hortonian runoff. In many cases, errors in runoff are nearly twice the magnitude of rainfall volume errors. Amplification of errors is larger at locations of small total rainfall volume.

Computing the actual values of the gradient of the atmospheric refractive index (as opposed to assuming a constant value) does not affect hydrologic outputs, provided that AP does not occur. Random noises that corrupt the radar measurement process, at least those considered in this study, have minor hydrologic impacts compared to the systematic range effects. Calibration errors can have a significant impact on predicted runoff.

At far ranges, radar measurements corrupted by calibration errors sometimes produce more accurate hydrologic outputs than error-free measurements. This makes identifying radar measurement errors more complicated and may lead to erroneous conclusions when radar measurements are compared to the measurements of other sensors.

Adjustment of radar-rainfall estimates by multiplying them by a bias factor to make the total rainfall volume match the "true" rainfall volume, as done in multisensor estimates, seems to provide acceptable runoff volume and hydrograph predictions at radar ranges below 100 km. At farther ranges, the predicted runoff and hydrographs have appreciable errors.

The simulation framework we present in this paper provides a useful tool for studying the problems of the hydrologic applications of weather radar data. In particular, we focus on the issue of radar-rainfall estimation uncertainty and the propagation of the errors through rainfall-runoff models. Our study admittedly has limitations. We only consider a single, convective storm and neglect the effect of bright band. We do not address the issues of radar

data quality control (such as anomalous echo detection and elimination). We only consider single parameter S-band radars. Still, despite these and other limitations, we demonstrate the utility of the simulation approach and consider the insight it provides. For example, we study the non-negligible effects of radar position (orientation) with respect to the basin, and we are able to isolate the quantitative effects of various radar-related sources of uncertainty. The significant level of some of these effects clearly indicates the need for more research on these issues. Such studies should include both simulation methods, such as the one we describe above, as well as real data-based studies. We hope that through collaboration between the relevant federal agencies and the research community we will be able to design and conduct appropriate field and data experiments. We believe that such experiments will ultimately lead to the improved predictive capabilities of hydrologic processes.

Acknowledgements The authors acknowledge the assistance of Dr. Emmanouil "Manos" Anagnostou of the University of Connecticut in adapting the radar simulator to function with ARPS output. This project was primarily funded by the U.S. Army Research Office through Young Investigator Grant DAAH04-96-1-0026 to the second author with a subcontract to the Iowa Institute of Hydraulic Research.

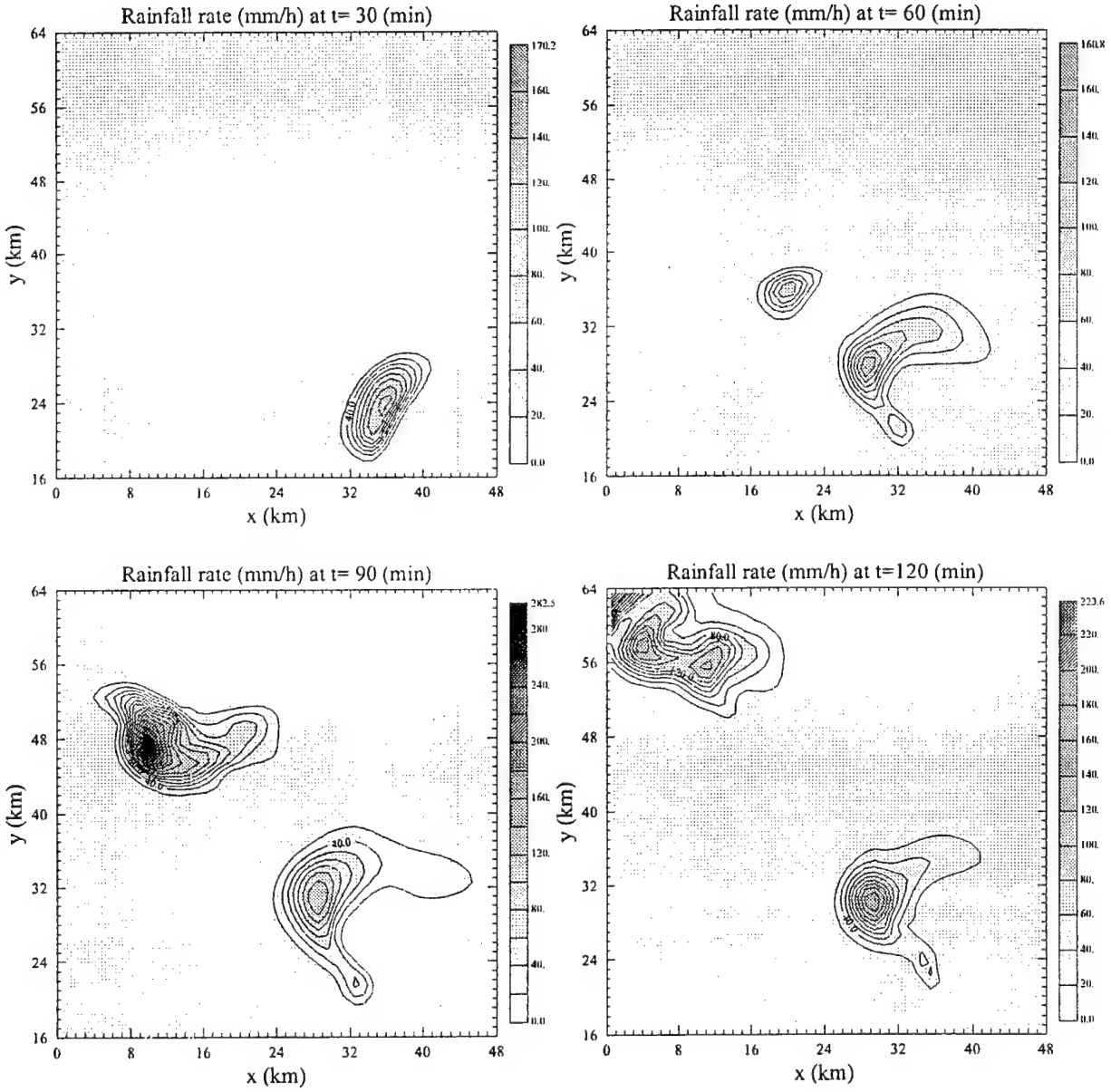
Rainfall rate (mm/h) at t= 30 (min)
Rainfall rate (mm/h) at t= 60 (min)
Rainfall rate (mm/h) at t= 90 (min)
Rainfall rate (mm/h) at t=120 (min)
y (km)
x (km)
64
56
48
40
32
24
16
0
8
16
24
32
40
48

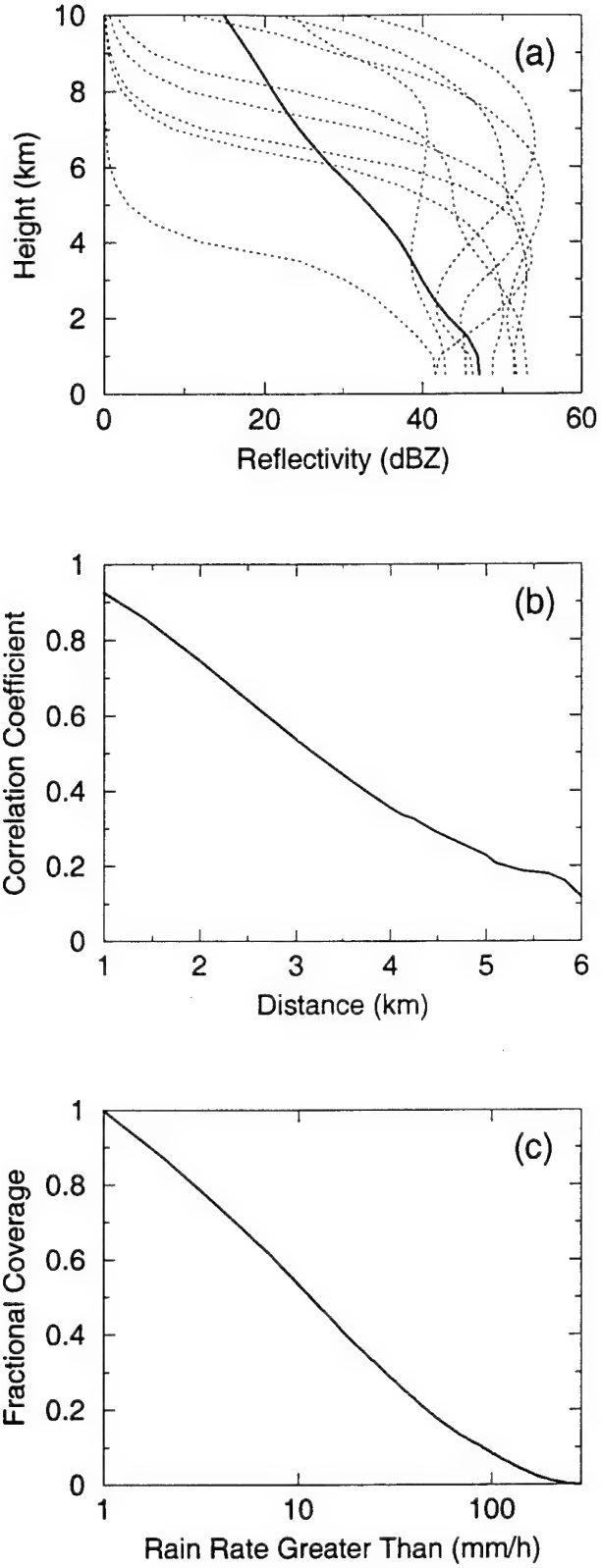
(a)
Height (km)
Reflectivity (dBZ)
0
2
4
6
8
10
0
20
40
60
(b)
Correlation Coefficient
Distance (km)
0
0.2
0.4
0.6
0.8
1
1
2
3
4
5
6
(c)
Fractional Coverage
Rain Rate Greater Than (mm/h)
0
0.2
0.4
0.6
0.8
1
1
10
100

Figure 2

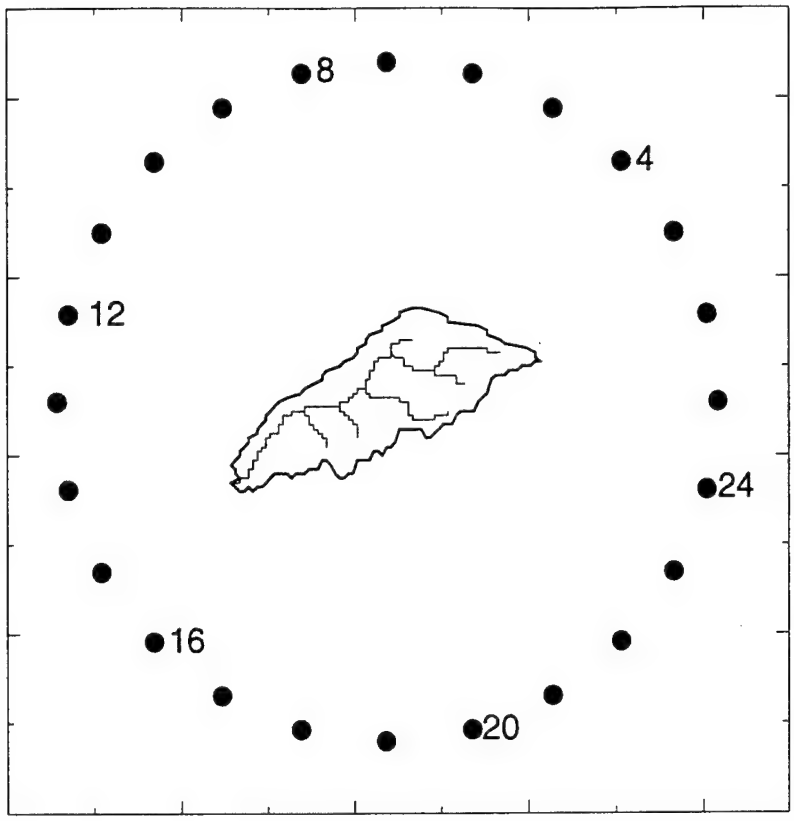

Figure 3

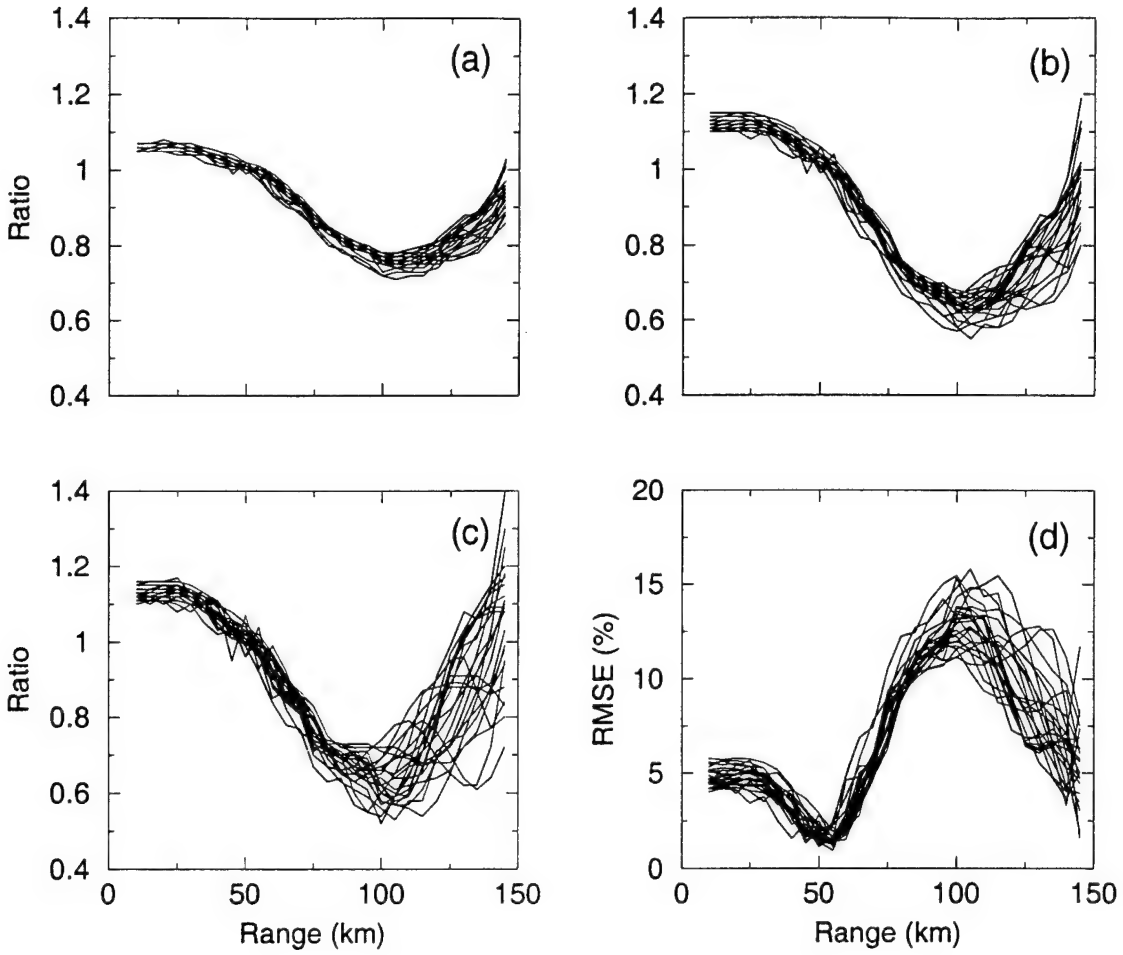
(a)
(b)
(c)
(d)
Ratio
Ratio
RMSE (%)
Range (km)
Range (km)
1.4
1.2
1
0.8
0.6
0.4
20
15
10
5
0
0
50
100
150

Figure 4

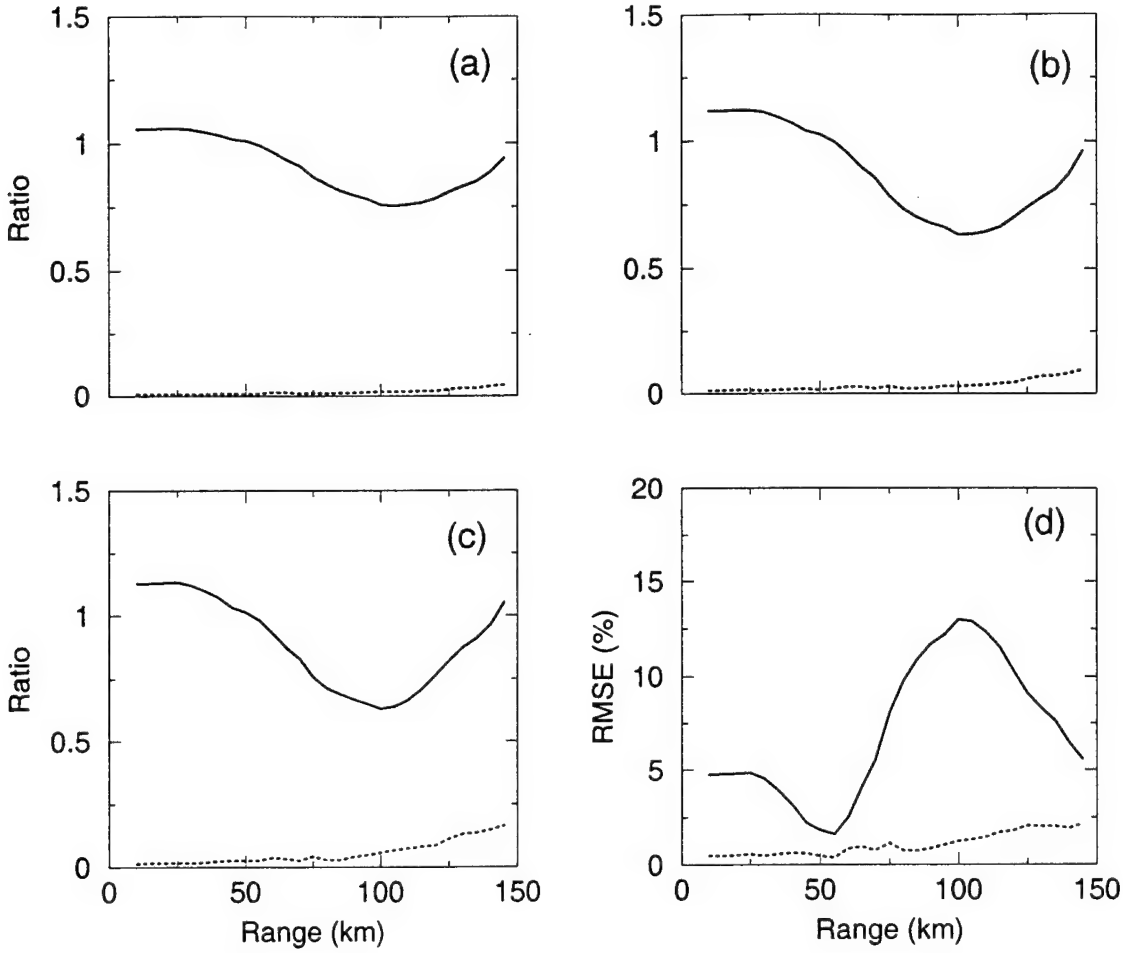
(a)
(b)
(c)
(d)
Ratio
Ratio
RMSE (%)
1.5
1
0.5
0
20
15
10
5
0
50
100
150
Range (km)
Range (km)

Figure 5

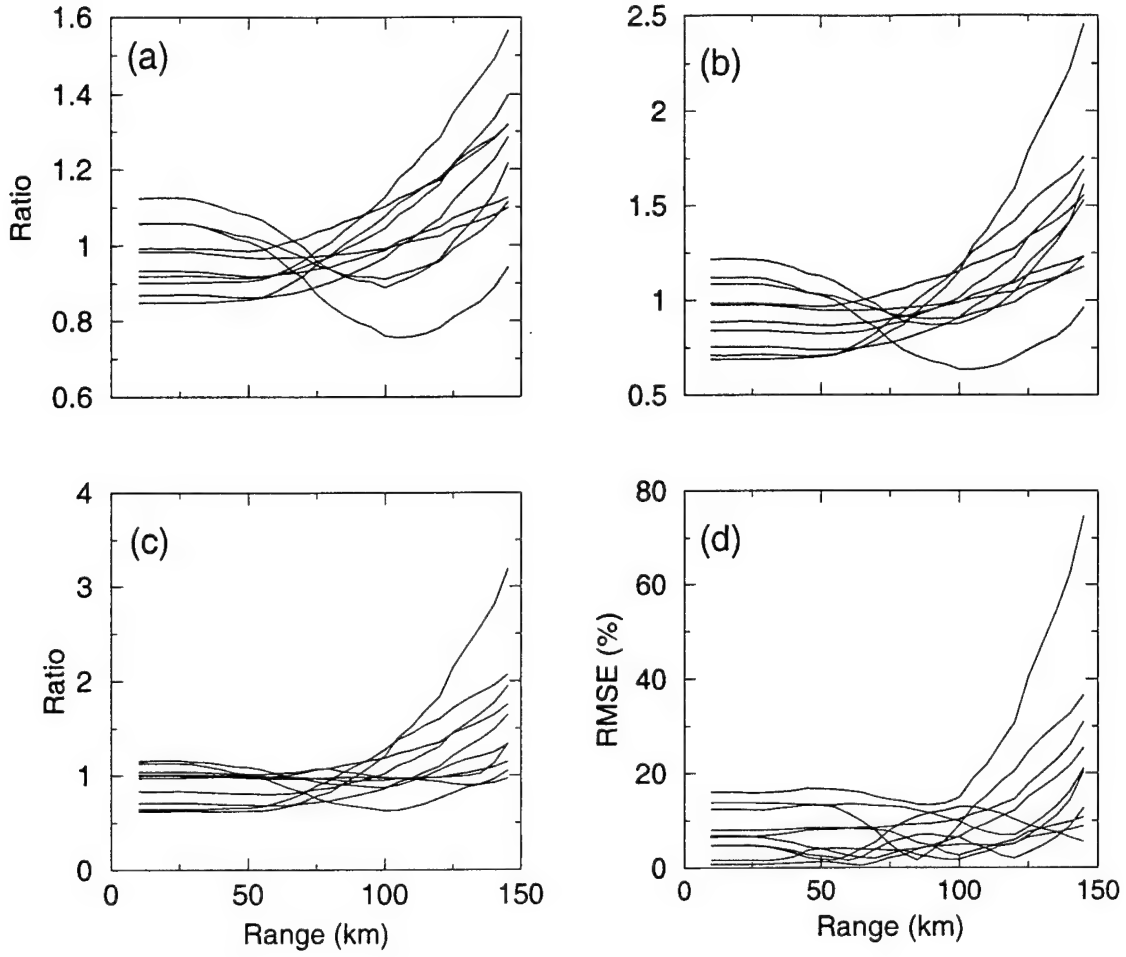
(a)
(b)
(c)
(d)
Ratio
Ratio
RMSE (%)
Range (km)
Range (km)
1.6
1.4
1.2
1
0.8
0.6
2.5
2
1.5
1
0.5
4
3
2
1
0
80
60
40
20
0
0
50
100
150

Figure 6

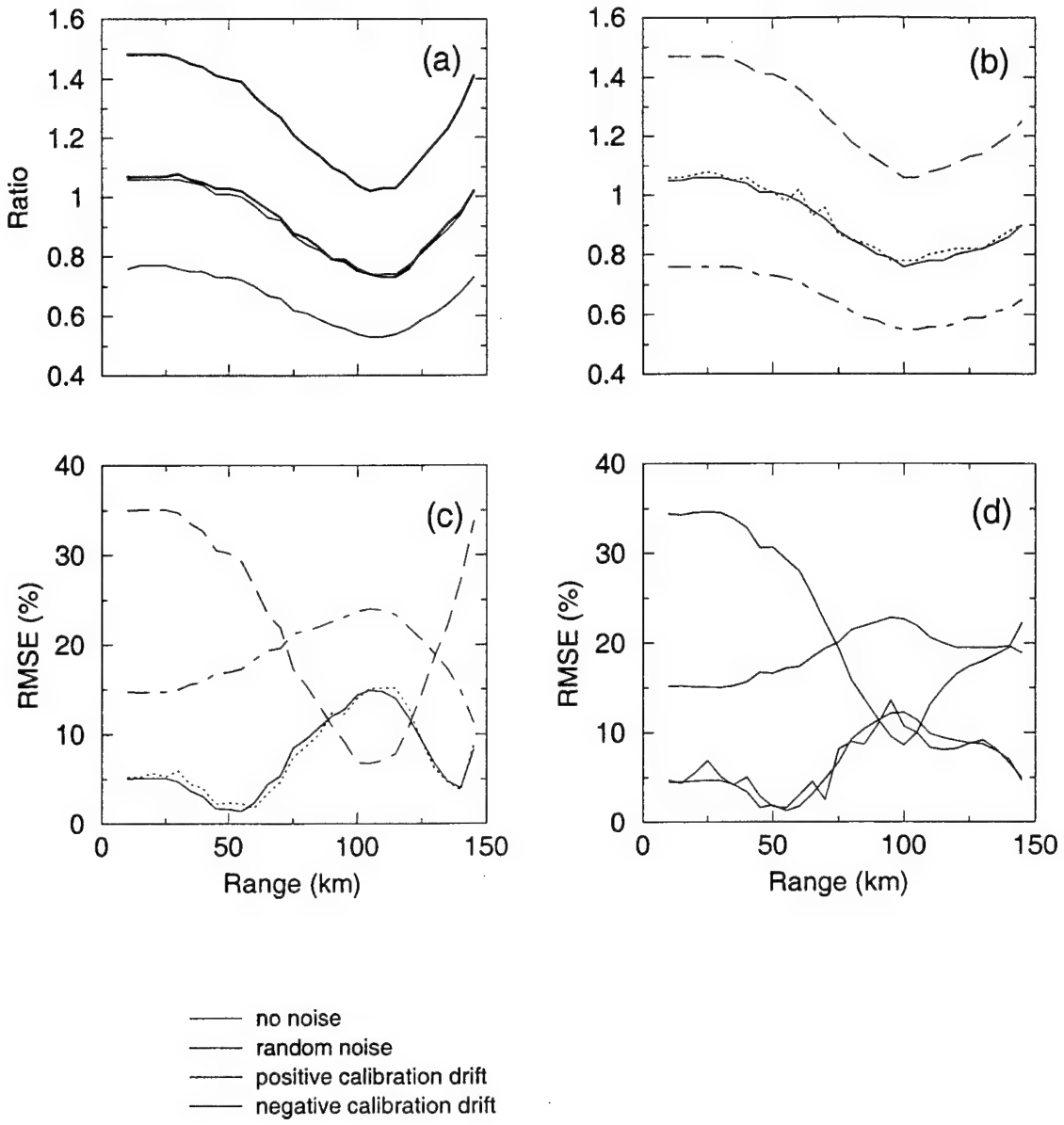
(a)
(b)
(c)
(d)
Ratio
RMSE (%)
Range (km)
1.6
1.4
1.2
1
0.8
0.6
0.4
40
30
20
10
0
0
50
100
150
no noise
random noise
positive calibration drift
negative calibration drift

Figure 7

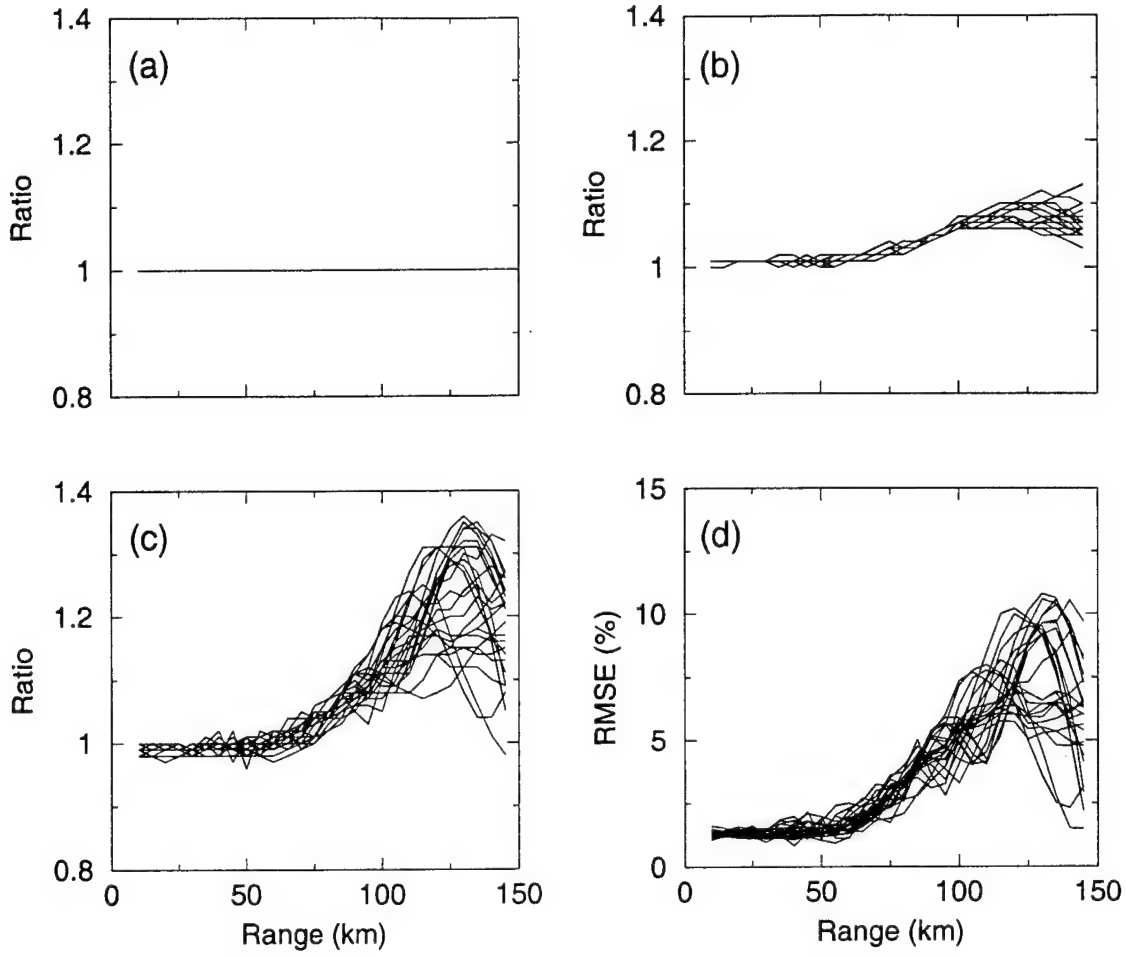

Figure 8

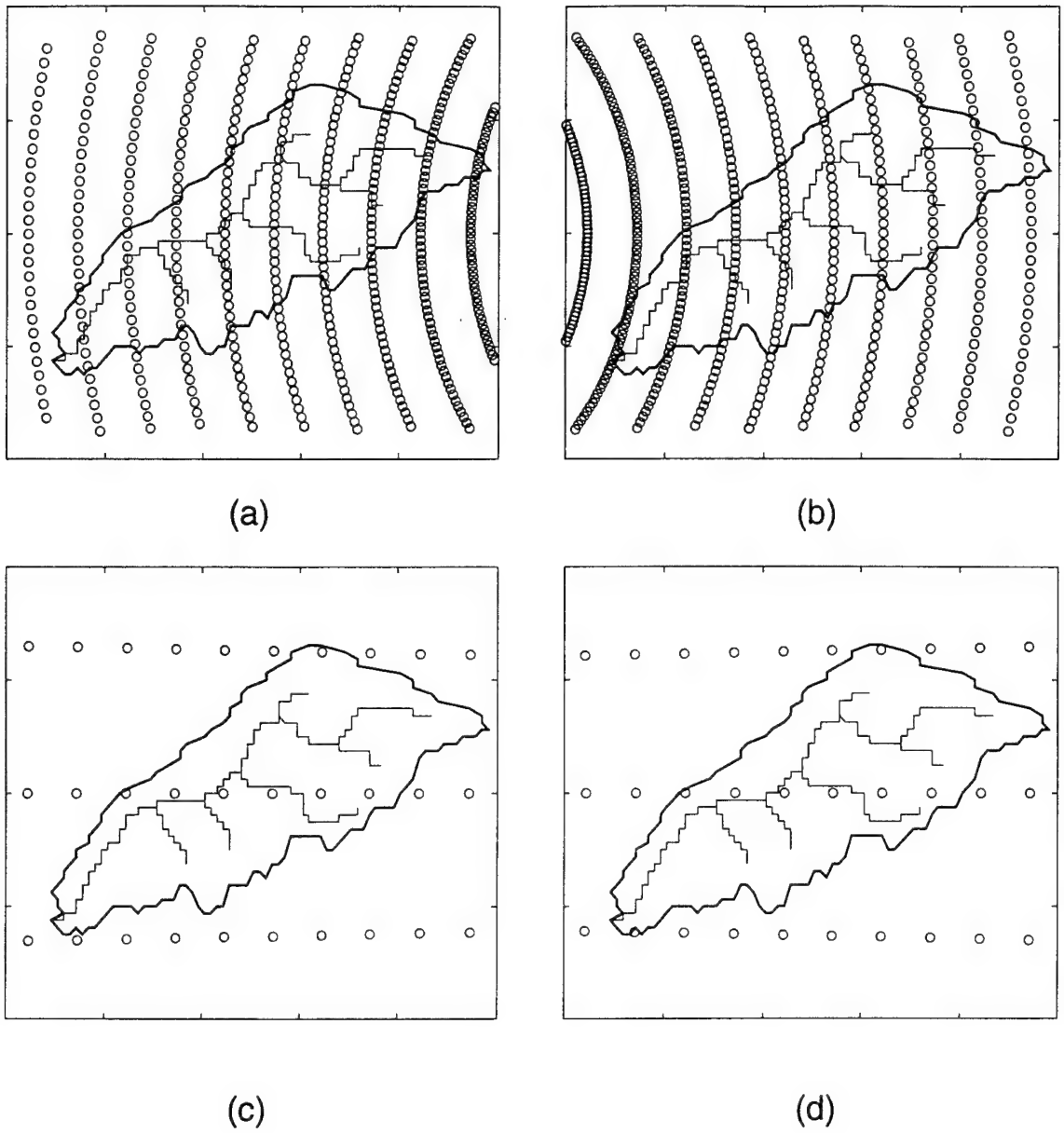

Figure 9

Location	ARPS Rainfall Volume (m^3)	Peak Discharge (m^3)	Runoff Volume (m^3)	Runoff Production Efficiency
1	1287741	104.8	766884	0.60
2	1230439	103.7	688193	0.56
3	803040	56.7	363803	0.45
4	828942	59.2	390689	0.47
5	689706	45.6	316993	0.46
6	450961	13.5	124478	0.28
7	475002	19.8	130138	0.27
8	789399	38.1	290071	0.37
9	1170596	93.3	650385	0.56
10	721109	35.0	287471	0.40

Table 2.1

3 STATISTICAL ANALYSIS OF RADAR-RAINFALL ERROR PROPAGATION

ABSTRACT

The prediction uncertainty of a hydrologic model is closely related to the uncertainty of its inputs and parameters. The most important challenges now are not whether we understand the theory and physics behind hydrologic processes but it is whether our model outputs match observed behavior or not and whether predictions from those models are meaningful and useful. In this paper we continue our investigation of the propagation of radar-rainfall estimation errors based on the simulation methodology developed by *Sharif et al.* [2001]. We investigate the propagation of radar-rainfall estimation errors through runoff predictions using a physically-based simulation methodology. The tools we use include a physics-based atmospheric model, a radar simulator, and a two-dimensional infiltration-excess hydrologic model. The spatial and temporal structure of the simulated three-dimensional precipitation field and the size of the study watershed allow us to develop a large set of rainfall events with different rainfall volumes and vertical reflectivity profiles and statistically analyze the propagation of rainfall error through runoff predictions. Rigorous statistical analysis of the relationship between estimated rainfall errors and characteristics of the predicted hydrograph is conducted for thousands of simulated events. In addition to the influence of radar estimation error, we study the relationship between event magnitude and the prediction error and its propagation. Furthermore, we apply Bayesian inference for

estimating the hydrologic output driven by radar-estimated rainfall based on statistical analysis of radar-rainfall error propagation.

3.1 Introduction

The scientific and technological advances of the past two decades have led to significant enhancements in understanding and modeling of hydrologic processes as well as in understanding and quantitative forecasting of precipitation e.g. emplacement of WSR-88D radar network and the development of automated algorithms and the deployment of a dual-polarization WSR-88D test bed; development of algorithms for computing precipitation intensity from satellite microwave reflectance data; development of storm-resolving models that use explicit microphysical parameterization and are initialized with fine scale radar and other observations; development of distributed hydrological and coupled meteorological-hydrological models based on physic and high resolution soil and terrain data [*Droegemeier et al*, 2000]. The focus of hydrologic modeling is shifting from how to solve and model mathematical equations and relationships of water flow to whether the predictions obtained from hydrologic models are meaningful and useful. The prediction uncertainty of a hydrologic model is closely related to the uncertainty of its inputs and parameters. *Spear and Hornberger* [1980] proposed a generalized sensitivity analysis approach (GSA) to identify critical uncertainties of a lake system modeled by a lake eutrophication model. The analysis starts by drawing a random set of values of the parameter under consideration. Monte-Carlo simulations will then follow and statistical analysis of the outputs will indicate the sensitivity of the system to that parameter and the uncertainty in the outputs corresponding to the

uncertainty of this parameter. Some recent methods addressing the prediction uncertainty of hydrologic model are related to GSA. The Generalized Likelihood Uncertainty Estimation (GLUE), a general framework for representing model parameter and prediction uncertainty within the context of Monte Carlo analysis coupled with Bayesian estimation and propagation of uncertainty [*Beven and Binley*, 1992; *Freer et al.*, 1996]. Monte Carlo Set Membership procedure [*Keesman*, 1990; *van Straten and Keesman*, 1991], the Prediction Uncertainty method [*Klepper et al.*, 1991], and the Multi Objective Generalized Sensitivity Analysis [*Bastidas et al.*, 1997] are all based on GSA. None of above studies addressed the uncertainty of distributed precipitation inputs to a hydrologic model.

The sources of uncertainty associated with prediction of runoff, both in terms of instantaneous discharge and total runoff, can also be decomposed into two sources: (1) input uncertainty associated with random inputs to the hydrologic model (2) and hydrologic uncertainty arising from all other sources e.g. model, parameter, estimation, and measurement errors [K*rzysztofowicz*, 1999]. Based on this decomposition of uncertainty, K*rzysztofowicz* [1993] developed a Bayesian predictive inference theory. It includes an input uncertainty processor, a hydrologic uncertainty processor, and an integrator. In the input uncertainty processor, the randomness of the input is represented by a density function. By simulating the input variables, and using a hydrologic model, a numerical distribution of the output variable (forecast variate e.g. runoff volume) is constructed. The induced density quantifies the uncertainty of the forecast variate. This is, in a broad sense, similar to Monte Carlo

simulation in other forecasting studies [e.g. *Lardet and Obled*, 1994].

3.2 Radar-Rainfall Estimation

One of the main factors affecting the accuracy of physically-based hydrologic simulations is rainfall input uncertainty. Rain gages suffer from undercatchment and a number of spatial and temporal sampling deficiencies. Although ground-based weather radars provide rainfall rate estimates over large areas at high spatial and temporal resolutions, radar data require vigorous quality control before being transformed into precipitation products that can be used as input to hydrologic models. The impact of radar-rainfall estimation errors on hydrologic predictions from physics-based models is an important area of study, with broad implications ranging from study of global climate change to watershed ecology and engineering hydrology.

A number of studies have focused on issues related to the applicability of radar-estimated rainfall in hydrologic modeling. *Kouwen* and *Garland* [1989] applied radar-estimated rainfall to a rainfall-runoff model based on hydrologically similar regions derived from remotely sensed land classification. In a study conducted by *Becchi et al.* [1994], simulated radar-rainfall maps were employed as input to a distributed hydrologic model to highlight the advantages of radar data of high spatial and temporal resolution. In a simulation study by *Schell et al.* [1992], in which several rainfall events were studied, they showed that

hydrographs obtained when using radar-estimated precipitation are far closer to the observed than those obtained when using precipitation from the single raingage located in the 8.13 km^2 basin of the study. This is similar to the conclusions of *Mimikou* and *Baltas* [1996]. Fewer studies addressed the issue of errors introduced to runoff predictions as a result of errors in radar precipitation. *Hudlow et al.* [1983] expected that errors in rainfall input to a nonlinear rainfall-runoff model would lead to even larger errors in the runoff predictions. *Collier* and *Knowles* [1986a, b, c] found that, for a given percent error in the precipitation estimation, an equal or lesser error in the predicted stream flow would result for some catchments; but in other circumstances the errors were amplified. They suggested that underestimating rainfall could be worse than overestimation, especially for large catchments. *Wyss et al.* [1990] concluded that errors in runoff predictions caused by errors of radar-estimated precipitation were likely to be less significant than the errors in the transformation from rainfall to runoff. *Pessoa et al.* [1993] showed that different widely accepted reflectivity-rainfall relationships resulted in significantly different hydrographs. They suggested that identification of appropriate reflectivity-rainfall relationship in real-time is necessary to produce reliable hydrologic forecasts. *Shah et al.* [1996] asserted that the use of spatially distributed precipitation was far more important when modeling a "dry" catchment than when modeling a "wet" catchment. Using the SHE model on a 10.5 km^2 basin, they also concluded that errors associated with lumping of the model processes outweighed errors from lumping of the rainfall. *Winchell et al.* [1997,1998] found that error in radar-rainfall estimates resulting from the use of inappropriate Z-R relationship resulted in equal or larger error in the resulting

runoff, regardless of runoff production mechanism.

3.3 Radar-Rainfall Estimation Error Propagation

Some researchers used physically-based simulations of the radar measurement process to study the radar-rainfall estimation error structure [e.g. *Krajewski and Georgakakos*, 1985; *Chandrasekar and Bringi*, 1987, 1988a, b; *Chandrasekar et al.*, 1990; *Krajewski et al.*, 1993; *Anagnostou and Krajewski*, 1997; and *Borga et al.*, 1997]. *Krajewski et al.* [1993] proposed a physically-based simulator of radar observables based on a two-dimensional stochastic space-time model of rainfall events and a statistically generated drop-size distribution. *Anagnostou and Krajewski* [1997] made several extensions to this simulator. The two-dimensional fields were complemented with a vertical structure of hydrometeors by choosing a cloud type model, which resulted in size, shape, and phase (mixed or single) distribution at discrete elevations. They simulated effects such as antenna beam pattern, horizontal and vertical gradients, atmospheric gases, and rain attenuation and represented the radar hardware noise by introducing random measurement errors. *Borga et al.* [1997] used the same tool to validate a bright band correction method.

Sharif et al. [2001] developed a simulation framework for the study of the hydrological impacts of radar-rainfall estimation errors. The simulation framework was physically based and consisted of an atmospheric model, a simulator of radar observations,

and a distributed hydrologic model. *Sharif et al.* [2001] coupled a physically-based atmospheric model of convective rainfall with an active microwave radiative transfer model to simulate radar observation of thunderstorms. They simulated a well-documented tornadic supercell storm that occurred near Del City, Oklahoma on 20 May 1977 using the atmospheric model ARPS developed at the Center for Analysis and Prediction of Storms (CAPS) at the University of Oklahoma [*Xue et al.*, 1995; *Xue et al.*, 2000a; *Xue et al.*, 2000b]. Radar observations of that storm were then simulated and used to evaluate the propagation of radar-rainfall errors through distributed hydrologic simulations. A modified version of the radar simulator developed by *Anagnostou and Krajewski* [1997] was used in that study. This physically-based methodology allows direct examination of the impacts of radar-rainfall estimation errors on land-surface hydrologic predictions and avoids the limitations imposed by the use of rain gage data. Results indicated that the geometry of the radar beam and coordinate transformations due to radar-watershed-storm orientation had an effect on radar-rainfall estimation and runoff prediction errors. In addition to uncertainty in the radar reflectivity vs. rainfall intensity relation, *Sharif et al.* [2001] reported significant range-dependent and orientation-related radar-rainfall estimation errors, which should be quantified in terms of their impact on runoff predictions. The methodology provides a tool to perform experiments to address some operational issues related to the process of radar-rainfall estimation and its use in hydrologic prediction. Using that approach, the authors were able to simulate several sources of radar measurement and estimation errors, both systematic and random and isolate the quantitative effects of various radar-related sources of

uncertainty.

3.4 Objectives

In this paper we continue our investigation of the propagation of radar-rainfall estimation errors based on the simulation methodology developed by *Sharif et al.* [2001]. We simulate a storm that covers a large area and we move the location of the study watershed within the storm domain to obtain different realizations of the storm over the watershed. We assume that the rainfall field generated by the atmospheric model, which is a realistic representation of a convective rainy atmosphere, is the ground "truth". We then run the radar simulator and use radar-estimated rainfall from the simulated storm as input to a calibrated (for a certain actual basin), physically-based, infiltration-excess, watershed model to analyze the propagation of radar-rainfall estimation errors. The spatial and temporal structures of the precipitation field, combined with use of 500 hundred locations within the storm domain, allow us to develop a large set of rainfall events with different rainfall volumes and vertical reflectivity profiles and analyze statistics of the "true" and estimated hydrologic outputs. In addition to the influence of radar range and radar orientation, we study the relationship between the rainfall event magnitude and the prediction error. Furthermore, we apply Bayesian inference for estimating the hydrologic output driven by radar-estimated rainfall based on statistical analysis of radar-rainfall error propagation.

3.5 Storm Simulation

The source of precipitation date in this study is the ARPS forecast at 500 meter spatial resolution, in all directions, for the 21-22 January, 1999 Arkansas tornado outbreak. The ARPS is a three-dimensional, nonhydrostatic compressible model formulated in generalized terrain-following coordinates. It contains a comprehensive physics package and a self-contained data analysis, radar data retrieval and assimilation system. The model has been subjected to real-time weather prediction testing over several regions since mid-90s. A comprehensive description of the formulation, numerical solution methods, physics parameterizations, computational implementation, and configuration instructions for the ARPS is given in *Xue et al.* (1995). More recent improvements and model verifications are described in *Xue et al.* (2000; 2001a; 2001b).

During the afternoon and evening of 21 Jan. 1999, a major tornado outbreak occurred in the state of Arkansas (AR). Fifty-six tornadoes were reported statewide with the strongest tornadoes rated F3 (maximum winds 71 ms^{-1} to 92 ms^{-1}) on the Fujita scale. Most of the tornadoes occurred between 4 and 11 pm CST, or between 2200 UTC Jan. 21 and 0500 UTC Jan. 22. Eight people were killed by the tornadoes. It is believed to be the largest tornado outbreak in Arkansas.

The synoptic-scale features and events of this case were documented in *Xue* [2001a], together with the ARPS model prediction results on nested 32-km and 6-km resolution grids.

Both grids successfully predicted the general precipitation area that is aligned along the southwest-northeast diagonal of the state of Arkansas. The set of precipitation on 6 km grid was delayed by as long as 4 hours, however, due primarily to inadequate spatial resolution, and because only explicit microphysics was used without cumulus parameterization. Prediction results were much improved when a 2 km grid is further nested within the 6 km grid. The 2km results were analyzed and compared with radar observations in *Xue et al.* [2001b]. These forecasts started from 1200 UTC, January 21, 8 hours before the first convective storms (about 2000) in Arkansas and about 10 hours before the first tornado (2200 UTC). For a 10 hour period starting from 8 hours into the model run (2000 UTC), a generally good agreement is found with respect to the number of storms in the state of AR, the rotational characteristics of storms, the speed and direction of storm-cell movement, the organization of initially isolated cells into lines and their subsequent propagation, the transition from a straight line into a mesoscale bow-shaped echo pattern, the reasonable timing of thunderstorm initiation and cessation of new cell development.

Specifically, at 2300 UTC Jan. 21, about a dozen storm cells can be identified both in radar observations and in the model, and both model and real storms exhibit isolated supercell storm characteristics with rotation more readily identifiable in the model (see Xue et al. 2001b). For the next three hours, from 2300 UTC Jan. 21to 0200 UTC Jan. 22, both observation and model showed new cells continually being generated at the south end of the convective line while older cells moved along the diagonal axis across the Arkansas state. By

the end of this three-hour period, the line in the model has turned more into the SW-NW orientation. As more cells were created through splitting process and the low-level cold pool spread, the storms became closer to each other and some started to join together, creating connected line segments.

In the two hours following 0200 UTC, the trend for the cells to merge and form a continuous line continued both in the model and in the real world. By 0400 UTC, the southern end of the primary line is two to three counties away from the southern state border. At 0600 UTC January 22, the end time for the 2-km model run, the convective line was moving (eastward) across the eastern Arkansas state border.

In the paper, we choose the period from 0200 UTC to 0430UTC, January 22 when the initial supercell storms have evolved into the precipitation line, located at the northeastern regional of Arkansas and southeast Missouri. We studied the fine scale features and spatial variabilities of precipitation and then further nested a 500-meter resolution grid inside the 2 km grid, centered over this region of precipitation. The model predicted instantaneous precipitation rates at 30-minute intervals are plotted in Figure 1.

3.6 Radar Estimation Process Simulation

We simulate the radar beam propagation with consideration of the radar beam

curvature relative to the Earth's curvature. The three-dimensional fields of rain computed by ARPS are used to compute the volume backscattering and extinction cross sections of hydrometeors [*Ulaby et al.*, 1981]. Although the radar simulator calculates the refractive index at each grid, a constant value of the refractive index slope was used because of the relatively small impact on the hydrologic model output [*Sharif et al.*, 2001]. We used the default WSR-88D Z-R relationship of $Z=300R^{1.4}$ [*Fulton et al.*, 1998], to covert reflectivities into rainfall rate estimates. We computed the attenuation of electromagnetic waves by rain from the radar as a function of the radar wavelength (10 cm), rainfall intensity, and distance between radar and hydrometeors. Attenuation by atmospheric gases, which is typically larger than rain attenuation for S band, is only a function of radar wavelength and distance [*Doviak and Zrnic*, 1993]. We did not model atmospheric gases attenuation assuming that it can be easily accounted for in real radar data processing systems.

We placed our virtual radar at 24 equi-spaced orientations (every 15°) around each watershed position tested. We also varied the distance between the radar and the center of the catchment along these directions, as illustrated in Figure 2. We placed the watershed in 500 different locations within the storm domain to obtain different cases of the radar estimation process because of the high variability of rainfall within the mesoscale convective complex. Justification for this radar-storm-watershed setting can be found in *Sharif et al.* [2001].

We ran the hydrologic model CASC2D [*Julien et al.*, 1995; *Ogden* 1998], using the "true" ARPS generated rainfall fields and radar-estimated rainfall fields. Comparison of hydrologic model outputs based the "true" rainfall and the radar-estimates-based ones was assessed by calculating four error statistics. These statistics are: the watershed total rainfall volume ratio, the root mean square error in simulated hydrograph, the simulated total runoff volume ratio, and the hydrograph peak discharge ratio.

The main simulations focus on the effect of range and orientation to highlight the spatial variability vertical rain water (or reflectivity) profile within the same storm and its impact on hydrologic model predictions. We did not conduct radar simulations above the freezing level although the atmospheric model included ice microphysics in its simulations. We computed probability densities of the "true" and radar-estimated hydrologic outputs from the sample of events simulated. We then transformed the distributions to normal distributions, using a power function, to simplify statistical modeling of the dependence between the two distributions. Assuming that the only source of uncertainty is the radar-estimated rainfall, we suggested a Bayesian approach for probabilistic estimation of hydrologic outputs derived by "uncertain" radar-estimated rainfall. We discuss ways to extend the approach to include more complex situations.

3.7 Radar-Storm-Watershed Setting

The purpose of the majority of the simulation runs is to develop a large sample of rainfall-runoff events in which the radar-rainfall errors are only caused by the effects of range and orientation between the radar and study watershed. For all watershed locations tested, the closest radar position used was 10 km from the center of the watershed. We then gradually increased the range at an increment of 5 km, up to 145 km from the center of the watershed. We limited the range to 145 km to avoid the influence of the freezing level on radar-measured reflectivity for the studied storm.

The influence of radar watershed orientation is examined by placing the radar at 24 equi-spaced orientations (every 15°) and varied the range along these directions as illustrated in Figure 2. The 28 range increments were the same for all 24 radar orientations in all watershed locations. The orientations were coded with numbers 1 through 24, orientation 1 being exactly east of the watershed center. We distributed the orientations over 360° because of the asymmetry of the simulated storm. "True" rainfall fields are input to the hydrologic model in grid format whereas radar-rainfall estimates are input to the hydrologic model in polar coordinates. We applied Thiessen Polygons to compute rainfall rates for each hydrologic model grid. The comparison "error" statistics were computed after each hydrologic model run.

The watershed used in this study for hydrologic simulations is the 21.2 km^2 Goodwin Creek experimental watershed located in north-central Mississippi. The USDA-ARS National

Sedimentation Laboratory has continuously monitored the watershed since 1981. *Alonso* [1996] provides a detailed description of the watershed. The elevation of the watershed ranges from 68 to 127 m. The main channel has an average slope of 0.004 [*Bingner*, 1996]. The grid size used in CASC2D to model the watershed is 125 m ×125 m, to minimize computing time yet adequately describe the spatial variability of topography, soil texture, and land use/land cover. The watershed characteristics, taken together with the predominance of fine soil textures, indicate that Hortonian runoff production mechanism [*Senarath et al.* 2000]. The hydrologic model CASC2D was rigorously calibrated on this watershed by *Senarath et al.* [2000] and thus we feel that the model represents the watershed's runoff processes with reasonable accuracy.

The rainfall volume error measure is the ratio between radar-estimated catchment total rainfall volume and the 'true' total rainfall volume predicted at the ground level by the atmospheric model. The measures of the influence of radar error on hydrologic model response are three of the statistics that are typically used to calibrate hydrologic models and evaluate their performance [e.g. *Brazil*, 1988; *Senarath et al.*, 2000]. Root mean square error percentage (RMSE%) is computed by:

$$RMSE\ \% = \sqrt{\frac{1}{N}\sum_{i=1}^{N}(q_i^{est} - q_i^{ref})^2}\ /\ q^{peak}\ \% \qquad (1)$$

Where q^{est} is the simulated discharge driven by radar-estimated rainfall and q^{ref} is the corresponding discharge resulting from the reference ARPS modeled rainfall i.e. we assume

the hydrograph produced using ARPS rainfall fields to be the reference hydrograph. N refers to the total number of hydrograph ordinates used in the analysis, while i is the index denoting individual hydrograph ordinates. q^{peak} is the 'true' peak discharge.

The error in the peak discharge is expressed as the ratio between the estimated peak discharge and the 'true' peak discharge. The error in runoff volume is similarly expressed as the ratio of the estimated and reference total runoff volumes.

3.8 Simulation Results

We computed rainfall and hydrograph error measures for all 500 rainfall-runoff events. For each radar range, errors were computed for 24 radar orientations, a total of 12000 values for each radar range. As found by *Sharif et al.* [2001], errors generally increase with radar range and errors in runoff volume and peak discharge are typically larger than the corresponding errors in rainfall volume. We show plots of probability density function (pdf) and cumulative distribution function (CDF) for the four error measures in Figures 3 and 4. We compare pdf and CDF curves for two radar ranges, 100 km and 145 km from the watershed center. All histograms of Figure 3 consist of 20 classes and small value on the edges of the histogram may not be visible in the plot. Taking this account will make it easier to compare different histograms.

Rainfall volume ratio pdf histogram, Figures 3a and 3b, appears approximately Gaussian and peaks around the value of 1.0 for both radar ranges. The range of storm total accumulated rainfall error values is relatively small, between 0.88 and 1.08 for the 100 km radar range and increases to .78-1.24 for the 145 km radar range. For both radar ranges, there is slightly greater tendency towards underestimation than overestimation. The 145 km radar range pdf curve, Figure 3b, is more flat and the difference in the statistical distribution of the errors for the two radar ranges can also be noticed in the CDF curves, Figure 4a.

It is clear from Figure 3c that rainfall errors are greatly amplified in predicted runoff although rainfall and runoff error pdf's are not significantly different. The runoff volume error pdf histogram is more flat and has a significantly larger range than the rainfall volume error pdf histogram, an indicator of the big difference in variance of the two distributions – compare Figures 3a and 3c. The amplification of error is the case for all 28 radar ranges considered. The amplification of error can also be seen in Figures 5a and 5c for two radar ranges. Comparing the two histograms of Figure 2c and Figure 2d, reveals that rainfall volume error variance increases with range - the 145 km radar range histogram is more flat with a wider range on both cases of underestimation and overestimation.

For all radar ranges, the error in hydrograph peak discharge is more pronounced than runoff volume error. Peak discharge error pdf and CDF figures are similar to those of runoff volume error except for a slight difference in flatness and bigger difference in the ranges of

values. The plot of runoff volume error vs. peak discharge error shows increased underestimation and overestimation in peak discharge as compared to runoff volume, Figures 5c and 5d. When the errors are very small, i.e. close to the value of 1 in both axes, the scatter of points is less and points are approximately evenly distributed around the 1 to 1 line. This is the case for both radar ranges. Figures 3e and 3f show that the range of peak discharge error values for the 145 km radar range is more than twice the range of error values for the 100 km range and the pdf curve is more flat. The same can be deduced by comparing CDF curves. Like the runoff error pdf, the peak discharge pdf shows a slight tendency towards underestimation.

As expected, the pdf histogram of the hydrograph rmse percentage was very skewed towards smaller values. This is because rmse percentage distribution is related to the distributions of runoff volume and peak discharge errors; both distributions peak near the value of 1.0. Figures 3g and 3h show that rmse percentage increases with radar range and the tail of the 145 km radar range pdf histogram is a lot more extended than that of the 100 km radar range histogram which is clearly demonstrated in the CDF plots of Figure 4d.

The fact that rainfall volume error is amplified in predicted runoff volume and that peak discharge error is typically larger than runoff error can be clearly seen in Figures 6a and 6b. For each rainfall volume error value, the value of the corresponding error in runoff volume is compared to find whether it is greater or less to identify it as amplification or

damping of the error. This information was used to construct the probability distribution of error amplification shown in Figures 6a and 6b. The same was done to construct Figures 6c and 6d using runoff volume and peak discharge error data. For the 100 km radar range in Figure 6a and both radar ranges in Figure 5c and 5d, we see that the probability is close to 0.5 when there are very small errors in rainfall volume, 5a, or runoff volume, 5c and 5d. It has to be stressed that it is possible that the ratio of the radar-estimated and 'true' total rainfall volume can be close to 1.0 and still the radar and actual rainfall fields are not identical. For the 145 km radar range, as seen in Figure 5b, it was found that when the error in rainfall volume is very small the runoff volume error was less than rainfall volume error in 70% of the cases. A detailed discussion on the existences of significant runoff volume errors even when radar and actual rainfall volumes are equal can be found in *Sharif et al.* [2001]. The spikes on the sides of the probability plots occur when the concentration of points is very sparse as seen in the plots of Figure 5.

An important factor that influences the magnitude of error in radar-estimated rainfall volume and its propagation through hydrograph predictions is the magnitude of the rainfall-runoff event. The value of radar-estimated rainfall volume and actual rainfall volume ratio is plotted against the actual rainfall volume in Figure 7a, which demonstrates that rainfall volume errors are generally larger for small rainfall events. This relationship between event size and error magnitudes also holds for the three hydrograph errors i.e. runoff volume error, peak discharge error, and rmse percentage. All plots in Figure 7 show the average error, from

all 24 orientations, for the radar range of 145 km. Plots for other radar ranges show similar trends. The plots are similar when we plot the maximum or minimum error value of the 24 orientations against the event magnitude for all radar ranges.

3.9 Uncertainty Analysis

Different methods for processing radar precipitation products have been aimed at finding the most appropriate approaches for extracting as much information as possible about the rainfall rate and its spatial distribution at the ground level. Many researchers have discussed the limitations of different approaches. In this and in a previous study [*Sharif et al., 2000*], we highlighted some range-related radar rainfall estimation errors in idealistic situations. We attempt here to statistically qualify the limitations of the hydrological application of radar rainfall in our experiment. We try to quantify the hydrologic uncertainty of radar rainfall in terms of probability distributions. At this moment we assume that our virtual radar, atmospheric model, and hydrologic model are perfect. This way we avoid the complexity of numerous sources of uncertainty. The only source of uncertainty assumed is the errors associated with radar estimation process discussed in this paper.

First we quantify the uncertainty of the predicted runoff volume and peak discharge at a certain radar range. The source of uncertainty is the interaction of radar beam geometry and vertical and horizontal variability of radar reflectivity (or rainwater mixing

ratio). In this analysis we use the average of all 24 radar orientations, at a given radar range, for each of the 500 rainfall runoff events. After normality test [*Salas et al.*, 1993] of the distribution of both radar-estimated and 'true' runoff data, we transformed the data distribution to normal distribution using Power Exponent Transformation [*Salas et al.*, 1993]:

$$Y = (X + c)^e \tag{2}$$

X is the original variable, Y is the transformed variable, e and c are parameters. A value of c = 0 and a value of e = 0.5 were found appropriate. We treat the normally-transformed 'true' and estimated runoff volumes and peak discharges as random variables, E and T, where E is the estimated runoff variable, i.e. runoff volume or peak discharge, and T being the 'true' variable. The CDF's of the radar-estimated normalized runoff volume and peak discharge at the radar range of 145 km are shown in Figure 8. The relationship between the random variables E and T is modeled by building a conditional density function f(e|t). For simplicity we compute the parameters of a linear function using data from all events:

$$\begin{aligned} E(E \mid T = t) &= at + b \\ Var(E \mid T = t) &= \sigma^2 \end{aligned} \tag{3}$$

In the left-hand side of Figures 9a and 9b we show a plot of the conditional mean of E for a given value of T. The plot of the conditional density f(e|t) for a value of t equal to the mean value calculated from our data is shown on the right-hand side of the figures. The normality of the conditional density is confirmed by the apparent linear relationship between E and T and by normality test of the residuals of the regression. Under the conditions of our

experiment, one can qualitatively characterize the worth of radar data by examining the parameters of the conditional density. A value of a close to 1.0 and a small value of b indicate that radar estimates are very close to the truth. On the other hand, the value of the variance (σ^2) is a measure of the uncertainty of the radar estimates. We remind the reader that we are using transformed runoff data so the variance of the original data is much larger than that shown in Figure 9. Furthermore, we only considered very few of the radar estimation/measurement errors, which is reflected in the values of a and b, 0.9818 and 1.669 for runoff volume and 0.9801 and -.0008 for peak discharge, respectively.

The conditional density function f (e|t) can be useful in many situations e.g. in modeling studies where accurate information on the actual runoff variables are not available or during real time modeling of flash floods. Suppose that in a certain situation we only have a probabilistic estimate of the actual runoff variable; in the discussion we will comment on how the distribution of T may be obtained. Furthermore, let us assume that the density of T, g, is normal, with or without transformation, with a mean value of μ and a variance of V^2 i.e.

$$\begin{aligned} E(T) &= \mu \\ Var(T) &= V^2 \end{aligned} \tag{4}$$

From Equations 3 and 4, the expected normally distributed density of E will be:

$$\begin{aligned} E(E) &= a\mu + b \\ Var(E) &= aV^2 + \sigma^2 \end{aligned} \tag{5}$$

Under conditions of normality and linearity and using Bayes Theorem, the conditional

density of T, when the estimated runoff volume or peak discharge is e, will be *h* with parameters:

$$E(T \mid E = e) = \alpha e + \beta$$
$$Var(T \mid E = e) = \Pi^2 \tag{6}$$

Where

$$\alpha = \frac{aV^2}{a^2V^2 + \sigma^2}$$
$$\beta = \frac{\mu\sigma^2 - abV^2}{a^2V^2 + \sigma^2}$$
$$\Pi^2 = \frac{\sigma^2V^2}{a^2V^2 + \sigma^2} \tag{7}$$

An example of the use of function *h* is shown in Figure 10. Equation 7 can be applied as follows: assumed that we have obtained an estimate of the rainfall data from the radar for a certain rainfall event. We run our hydrologic model, assumed to be perfect, to estimate the runoff from this event. We also have an assumed density function of the actual runoff for the event, Equation 4; an alternative to this suppose we have an estimate of the density of 'true' rainfall and use the hydrologic model, assumed to be perfect here, to obtain an estimate of the 'true' runoff volume or peak discharge. We can then apply Equation 7, based on Bayes Theorem, to obtain a conditional density of the true runoff volume or peak discharge based on information in Equation 4 and updated by information obtained from the conditional density function of Equation 3. From Equation 7, it is clear that Π^2 is always less than V^2 and less than σ^2. The conditional mean of T for a given value of E is shown in the left-hand side of Figures 10a and 10b. On the right-hand side of the figure, the density *g* and the conditional

density $h(t|e)$ are plotted. In Figure 10a we assumed a value of μ equal to the mean value of the transformed 'true' runoff volume, 656 $(m^3)^{0.5}$, and assumed value of e of 646 $(m^3)^{0.5}$. The values of μ and e in Figure 10b are 7.62 $(m^3/s)^{0.5}$ and 7.42 $(m^3/s)^{0.5}$, respectively. But in reality the value of μ depends on the situation and it can or can not be very close to the observed value of E.

3.10 Discussion

Our simulation study reveals that it is very difficult to obtain an accurate estimate of rainfall rate and spatial distribution using radar estimates even if we assume that the radar is error free. It is also very difficult to make accurate corrections for radar range errors because the vertical profile of reflectivity is not constant within a storm. This is also true in real world applications and the relationship between radar estimate and more accurate estimates e.g. from a dense rain gauge network varies from event to event. This applies to radar-estimated rainfall and other driven hydrologic variables e.g. the estimated peak discharge can be significantly different from the actual measurement of peak discharge for the event which represents the 'true' peak discharge. This makes the use of conditional densities that relate the true and estimated hydrologic variables more realistic. Information from all events for which acceptable radar estimates and actual or quasi-actual measurements exist can be used to build the conditional density function that can be linear or non-linear. If the hydrologic variable is runoff volume or peak discharge, a hydrologic model is used and the output from

the hydrologic model using radar data will be compared to actual values of the hydrologic variable, e. g. measured values. There might be other sources of error that make it reasonable to express information from radar estimates in the form of probabilistic distributions rather than taking the estimate as the best available information. This applies to good quality radar data only because poor data might produce erroneous correlations. The conditional density can also be assessed subjectively by the modeler and does not have to be entirely based on real observations. One example of this is to use data from one watershed to modify the values of the parameters of Equation 3 based on data from another watershed, or use data from simulation studies to complement real data.

The normal transformation of data is not necessary but will make application of the Bayesian approach simpler. The dependant variable in the conditional density can be the 'true' or estimated hydrologic variable. If information on the actual hydrologic variable is to be updated by the observed estimates, the independent variable in the conditional density *f* has to be the 'true' variable. The values of the parameters of Equation 3 are specific to this simulation study and do not represent the actual relationship between radar estimates and actual observation at the radar range of 145 km. Using actual radar data, one would expect that parameter a to be significantly different than 1.0 and the variance to be significantly higher than the one computed in this study. In this study the relationship between E and T depends on the magnitude of the rainfall event, Figure 5. This violates the assumption of

stationarity of mean and variance in the conditional density. One way to handle this problem is to use different conditional densities for different ranges of event size.

Equation 5 uses information about the relationship between e and t, Equation 3, and the expected distributions of the hydrologic variable, Equation 4. The choice of the parameters of Equation 4 might depend on the discretion of the modeler and/or the situation. It can be computed statistically from previous data for similar events and/or from simulation studies of similar storms e.g. in this experiment we calculated parameters using information from different locations from the same storm. Applying the judgment of the modeler may be necessary for choosing the appropriate value of the variance in Equation 4. If the modeler assumes that he has no information about the value μ in Equation 4, by simply using $t = \alpha e + \beta$, the first part of Equation 6 reduces to the first part of Equation 3 with t on the left-hand side. In practical situations the value of μ can come from radar data assimilation or nowcasting using an atmospheric model and the variance V^2 may represent the reliability of the nowcasting method. In the worst case, construction of the density described in Equation 4 presents a rational statistical approach to utilize the qualitative knowledge of the modeler.

Treating the uncertainty of radar data and its hydrologic outputs within a probabilistic framework and application of Bayes theorem may not only have potential for practical utility at the present time, but it also presents an intellectual exercise for studying the uncertainty and reliability of hydrologic applications of weather radar. In some situations, the only available

data about a rainfall event is from weather radar. When using this data in modeling studies, it will be useful to quantify the associated uncertainty. Extreme events observed by radar only can be used for design purposes or in flood frequency analysis if the associated uncertainty is well understood. Instead of depicting radar products are reliable or not, it is reasonable to explicitly account for their uncertainty and the risks associated with their use.

In this study we treated the hydrologic uncertainty of radar data in a simplified manner. Actually, the same approach can be applied to treat the uncertainty of radar rainfall estimates and the uncertainty of the hydrologic model separately and then integrate the two uncertainties. The radar-rainfall uncertainty itself can be separated to measurement uncertainty and uncertainty stemming from rainfall averaging and grid size. In this experiment we could add an uncertainty in the radar estimates coming from sources other than the ones we discussed such that the radar estimated E would have a probability distribution. The conditional density of Equation 6 would then be integrated with the uncertainty of E to produce a distribution of T that integrates all uncertainties. In this study we combine all certainties associated with radar data and treated them as one hydrologic uncertainty. The approach can be extended to analyze the uncertainty of distributed inputs and outputs e.g. spatially variable rainfall uncertainty. The approach can also incorporate multiple interacting sources of uncertainties e.g. when output from one system serves as input to another.

3.11 Summary And Conclusions

We presented a simulation framework for studying the propagation of radar rainfall estimation errors in predicted runoff. We used a state-of-the-art atmospheric model to simulate a storm that covers a large domain. The size of the study watershed made it possible to build a large data set of rainfall-runoff events. The variability within the storm allows us to treat the data set collected from different locations within the same storm as a surrogate to data sets compiled from different storms. We used a hydrologic model that had been rigorously calibrated on a well-monitored experimental watershed. The radar simulator used was adequate for simulating the errors addressed in this study and the simulated storm serves as an appropriate example of convective storms, at least for the purpose of modeling studies. We simulated pure radar orientation and range errors although the methodology makes it possible to incorporate many other systematic and random errors associated with radar-rainfall estimation process. The choice of our simulation tools and the simplicity of the errors we addressed allowed us to focus on statistical properties of errors and their propagation rather than the uncertainty associated with the modeling tools.

Frequency analysis of radar-rainfall errors revealed useful information about the statistical distributions of these errors and their propagation. The inferred statistical distributions represent only the storm analyzed in our experiment and actual distributions using real data might be significantly different. We expect the errors to be larger for real radar data and the mean values of errors to be significantly different than 1.0, especially at far

radar ranges. Our experiment also reveals that rainfall errors were typically magnified in predicted Hortonian runoff. Generally, peak discharge errors were larger than runoff volume errors. The relationship between rainfall volume error and hydrograph errors depends on the size of the rainfall event, which complicates the analysis of this relationship. The findings of this study are not restricted to radar-estimated rainfall error propagation, but the shape and size of the watershed might have played an important factor in the details of findings of the study.

We tried to quantify the uncertainty of hydrologic applications of weather radar in the form of probability densities. The conditional density of a radar-observed hydrologic variable for a given 'true' value of the variable, or vice versa, can be very useful in modeling studies and have potential for practical applications. Application of Bayes Theorem makes it possible to quantify the uncertainty of the 'true' hydrologic variable, based on radar-estimated data, in terms of a probability distribution, conditional on all available data and knowledge and expertise of the modeler. The approach can be applied to quality-controlled radar data from different storms at a certain watershed. Even quality-controlled radar precipitation errors might contain errors that are larger than the ones addressed in this study, e.g. effects of Anomalous Propagation and presence of 'bright bands'.

We acknowledge the limitations of this study, but the methodology can be extended for more rigorous radar data error studies. For example, we treated rainfall and runoff errors

at the watershed scale, but choosing a finer spatial scale might be more appropriate in many situations, especially for watersheds of larger sizes. The uncertainty associated with the modeling tools can also be integrated in the total uncertainty, which we did not include in this study. With all these limitations, we only mentioned a very few, we tried to demonstrate the utility of our methodology and its potential for practical application. We believe that these types of studies will help in understanding the uncertainty of hydrologic applications of weather radar and will prove to be very useful in making operational decisions based on radar products.

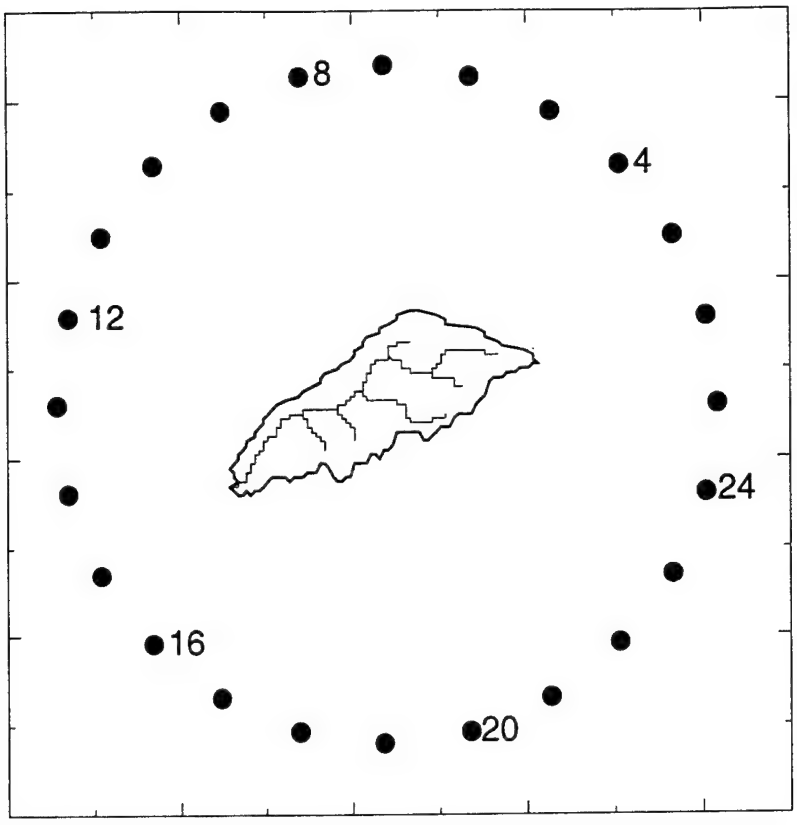

Figure 2

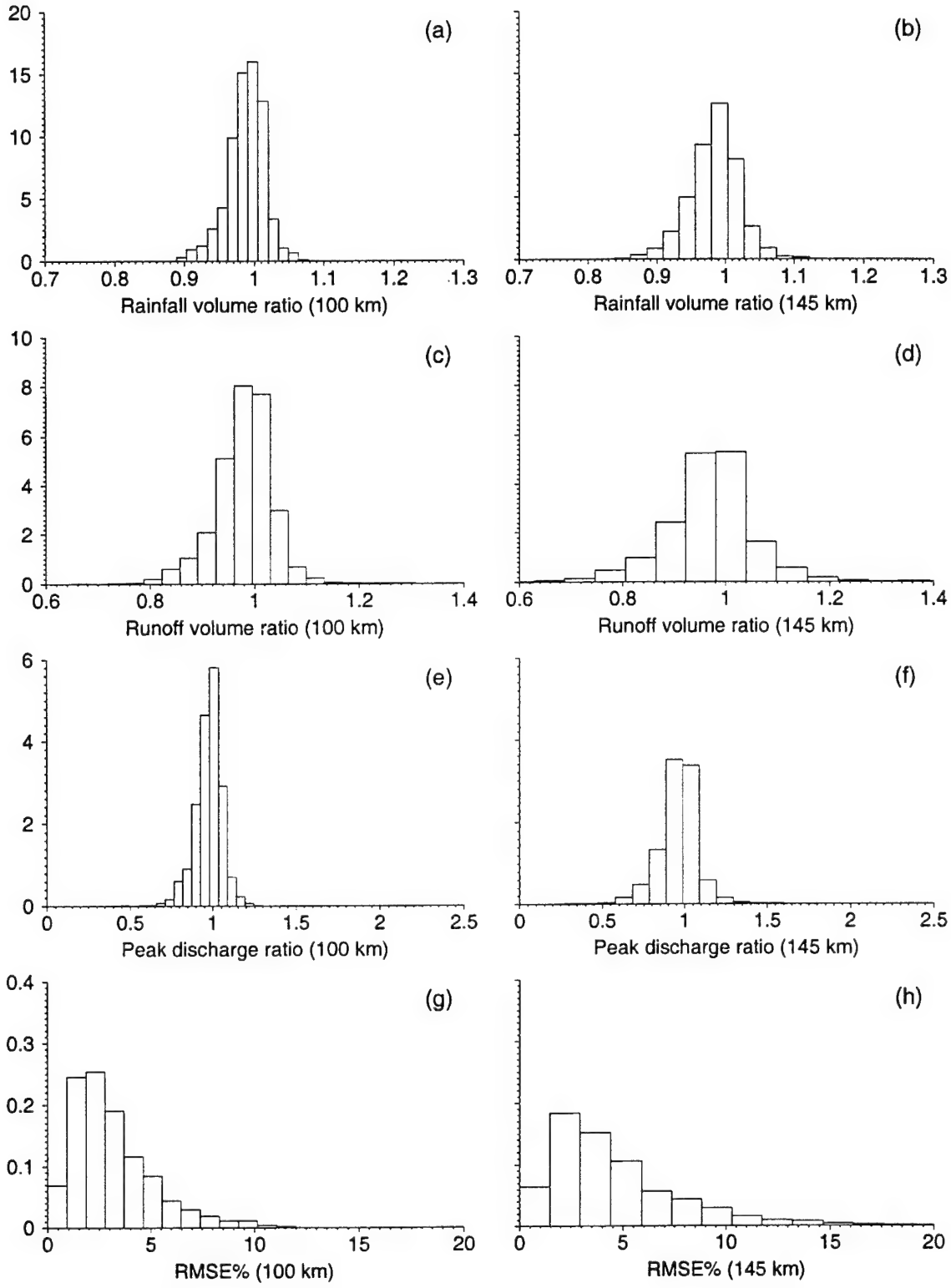
(a)
Rainfall volume ratio (100 km)
(b)
Rainfall volume ratio (145 km)
(c)
Runoff volume ratio (100 km)
(d)
Runoff volume ratio (145 km)
(e)
Peak discharge ratio (100 km)
(f)
Peak discharge ratio (145 km)
(g)
RMSE% (100 km)
(h)
RMSE% (145 km)

Figure 3

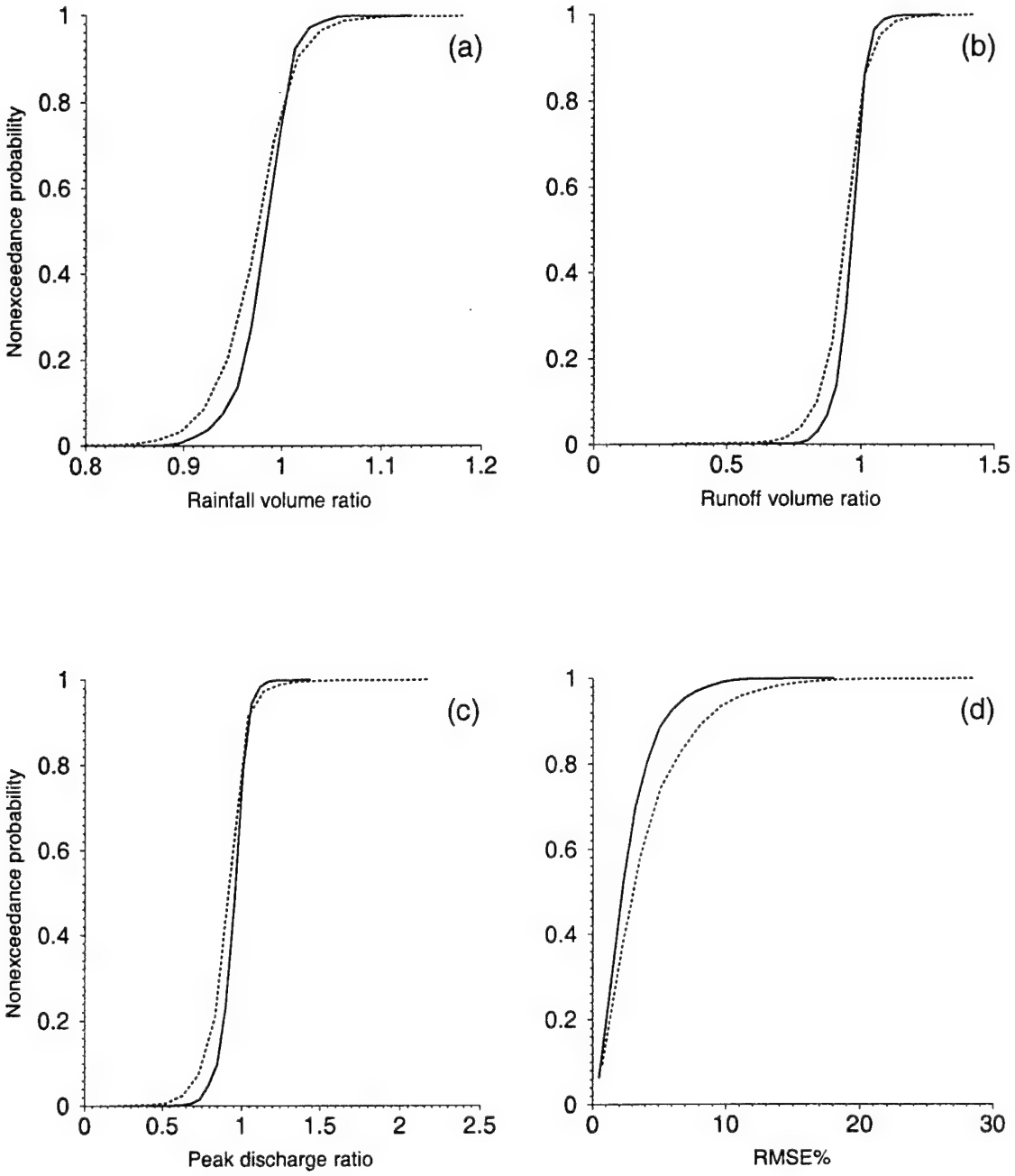
(a)
(b)
(c)
(d)
Nonexceedance probability
Rainfall volume ratio
Runoff volume ratio
Peak discharge ratio
RMSE%
0
0.2
0.4
0.6
0.8
1
0.8
0.9
1
1.1
1.2
0.5
1.5
2
2.5
10
20
30

Figure 4

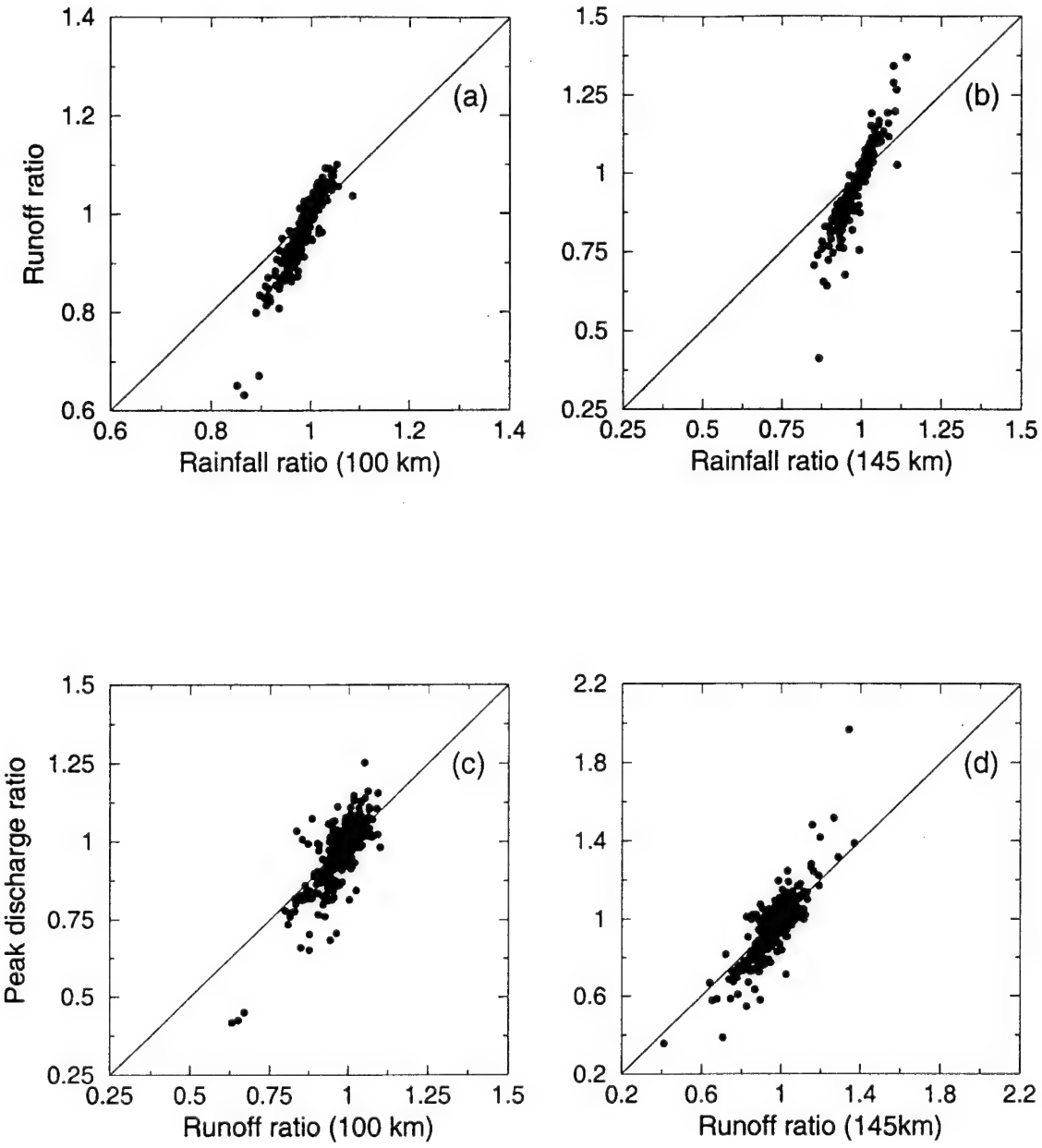
Runoff ratio
Rainfall ratio (100 km)
(a)
Rainfall ratio (145 km)
(b)
Peak discharge ratio
Runoff ratio (100 km)
(c)
Runoff ratio (145km)
(d)

Figure 5

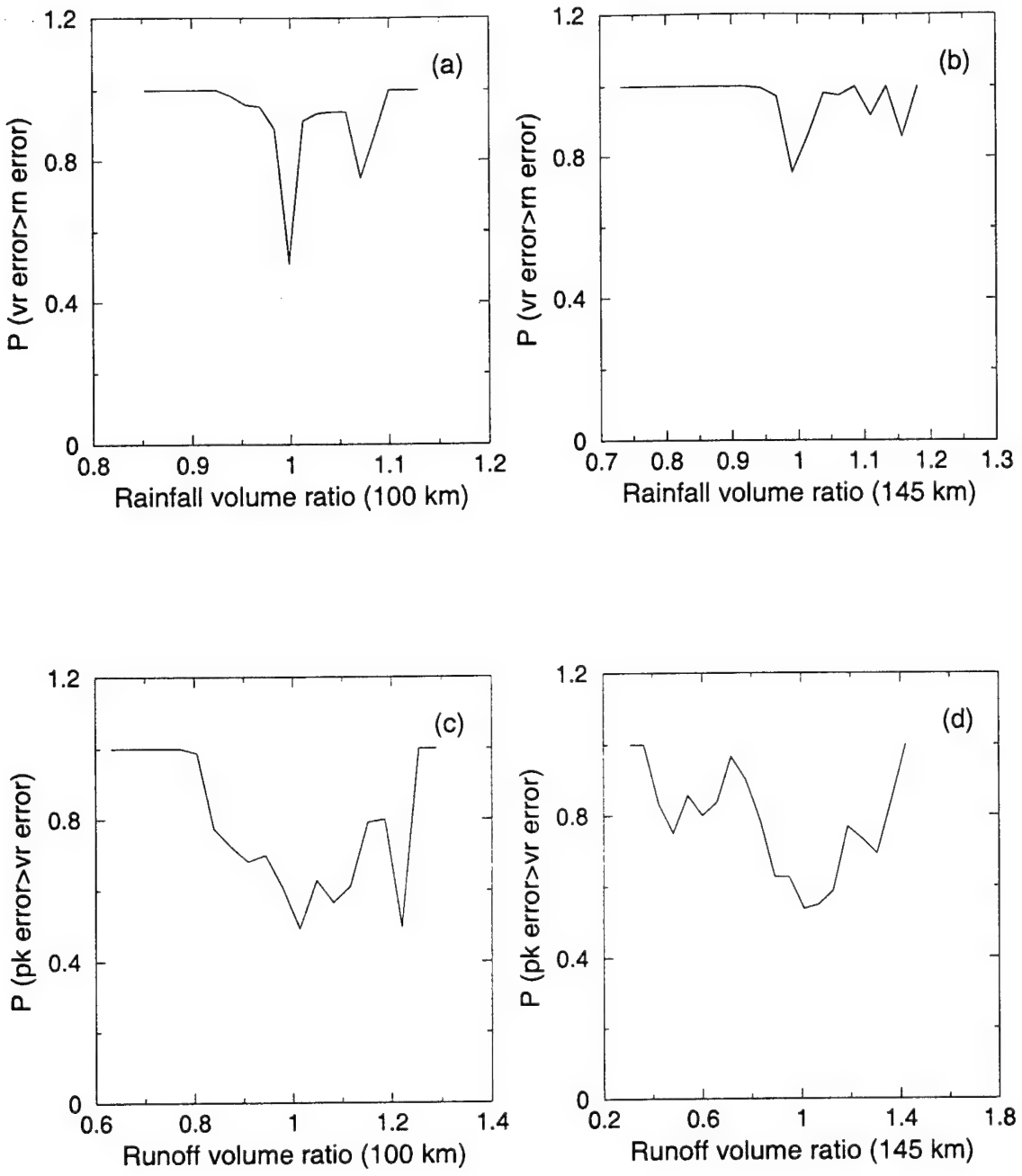
(a)
P (vr error>rn error)
Rainfall volume ratio (100 km)
(b)
P (vr error>rn error)
Rainfall volume ratio (145 km)
(c)
P (pk error>vr error)
Runoff volume ratio (100 km)
(d)
P (pk error>vr error)
Runoff volume ratio (145 km)

Figure 6

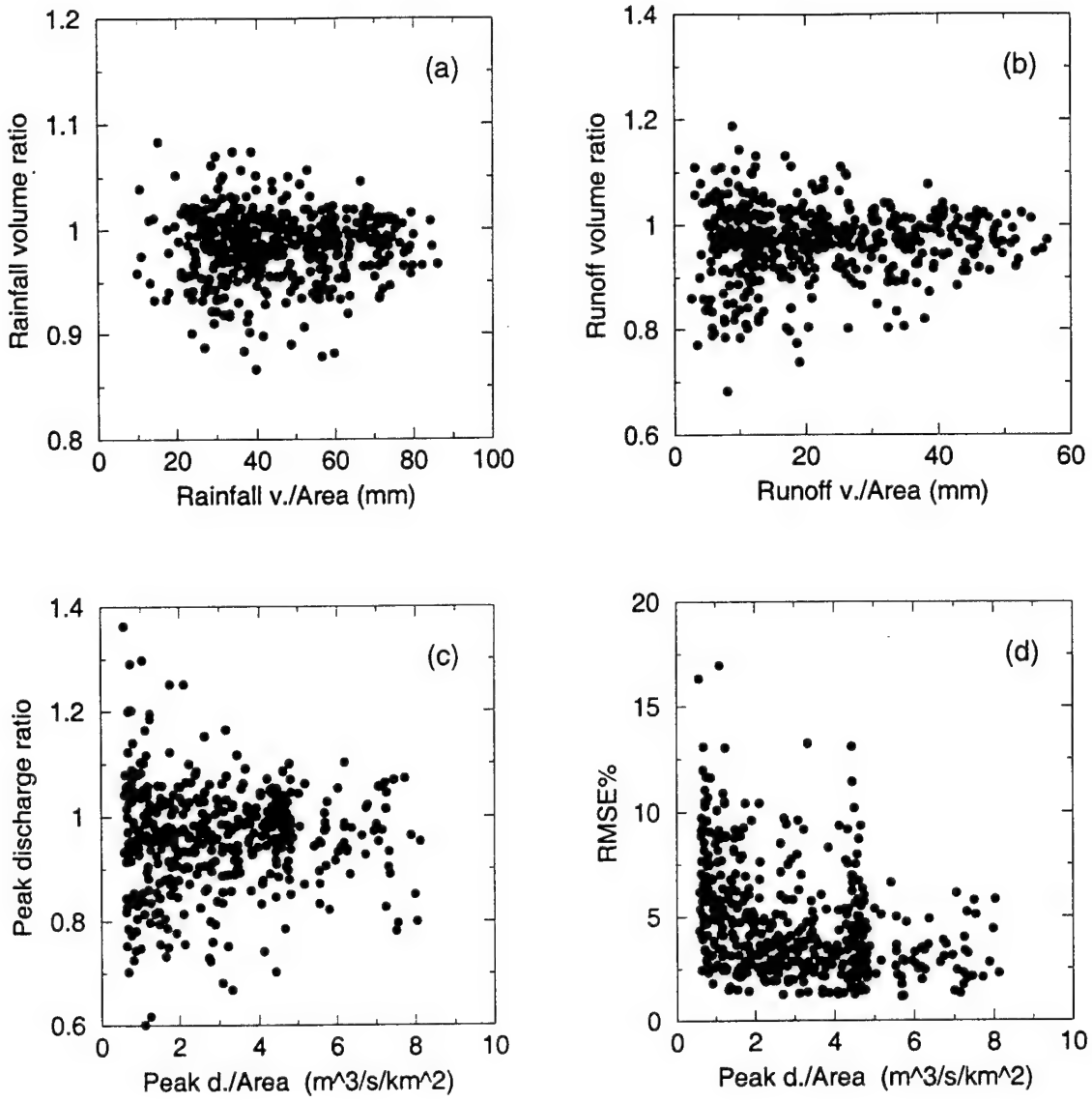
(a)
Rainfall volume ratio
1.2
1.1
1
0.9
0.8
0
20
40
60
80
100
Rainfall v./Area (mm)
(b)
Runoff volume ratio
1.4
1.2
1
0.8
0.6
0
20
40
60
Runoff v./Area (mm)
(c)
Peak discharge ratio
1.4
1.2
1
0.8
0.6
0
2
4
6
8
10
Peak d./Area (m^3/s/km^2)
(d)
RMSE%
20
15
10
5
0
0
2
4
6
8
10
Peak d./Area (m^3/s/km^2)

Figure 7

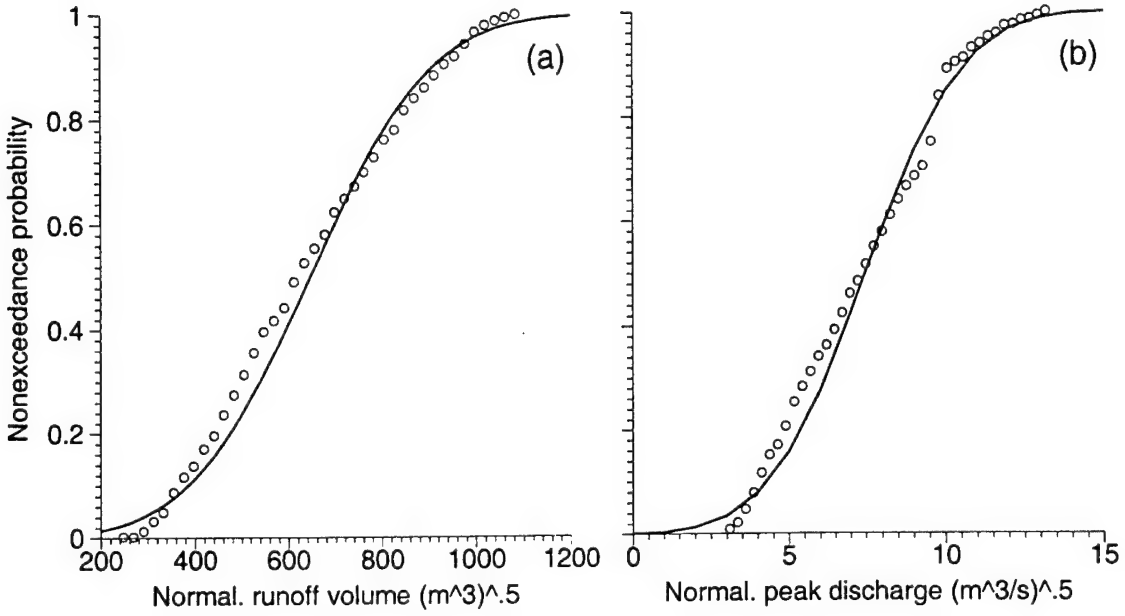
Nonexceedance probability
1
0.8
0.6
0.4
0.2
0
200
400
600
800
1000
1200
Normal. runoff volume (m^3)^.5
(a)
0
5
10
15
Normal. peak discharge (m^3/s)^.5
(b)

Figure 8

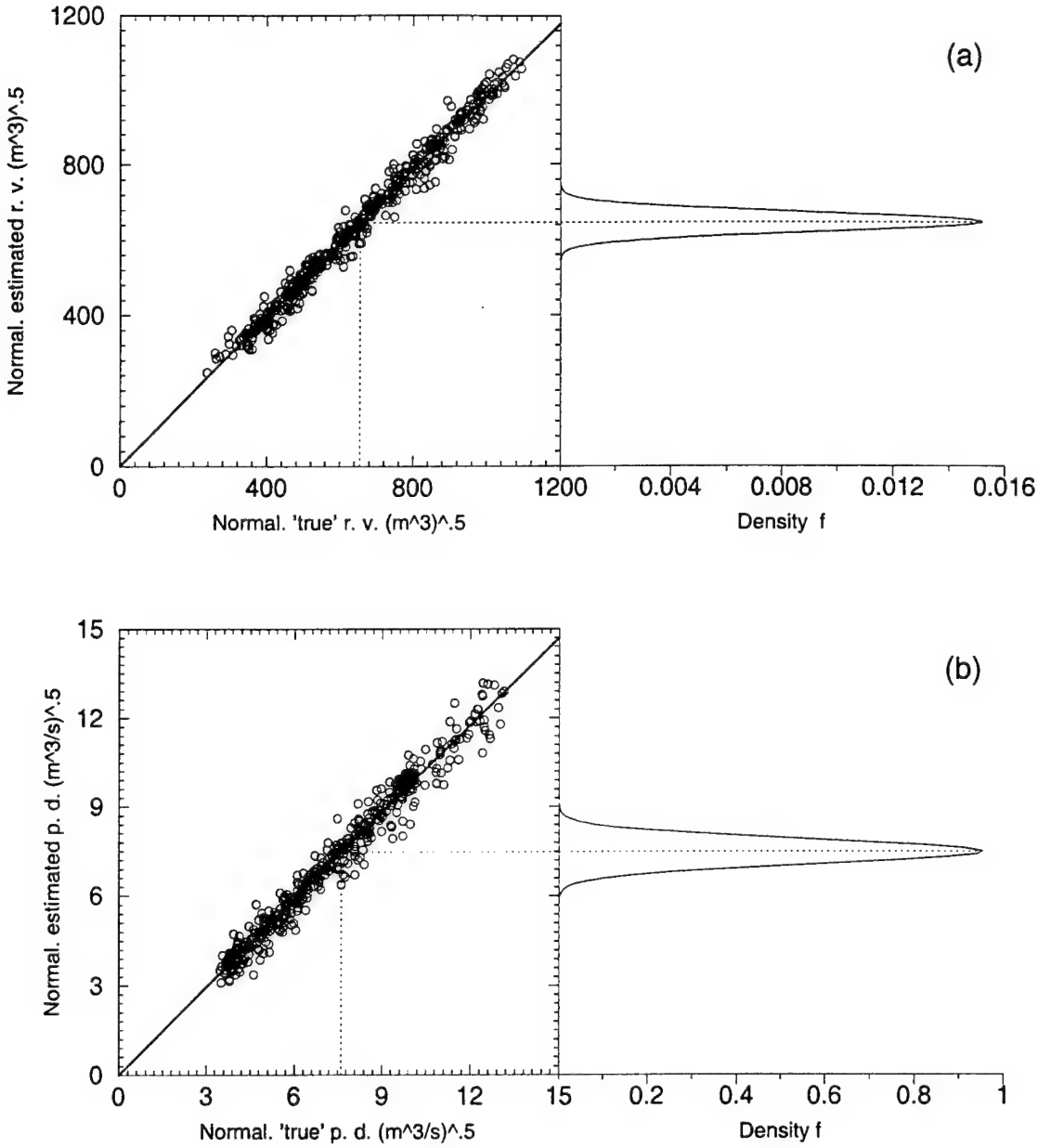
(a)
Normal. estimated r. v. (m^3)^.5
1200
800
400
0
0
400
800
1200
Normal. 'true' r. v. (m^3)^.5
0.004
0.008
0.012
0.016
Density f
(b)
Normal. estimated p. d. (m^3/s)^.5
15
12
9
6
3
0
0
3
6
9
12
15
Normal. 'true' p. d. (m^3/s)^.5
0.2
0.4
0.6
0.8
1
Density f

Figure 9

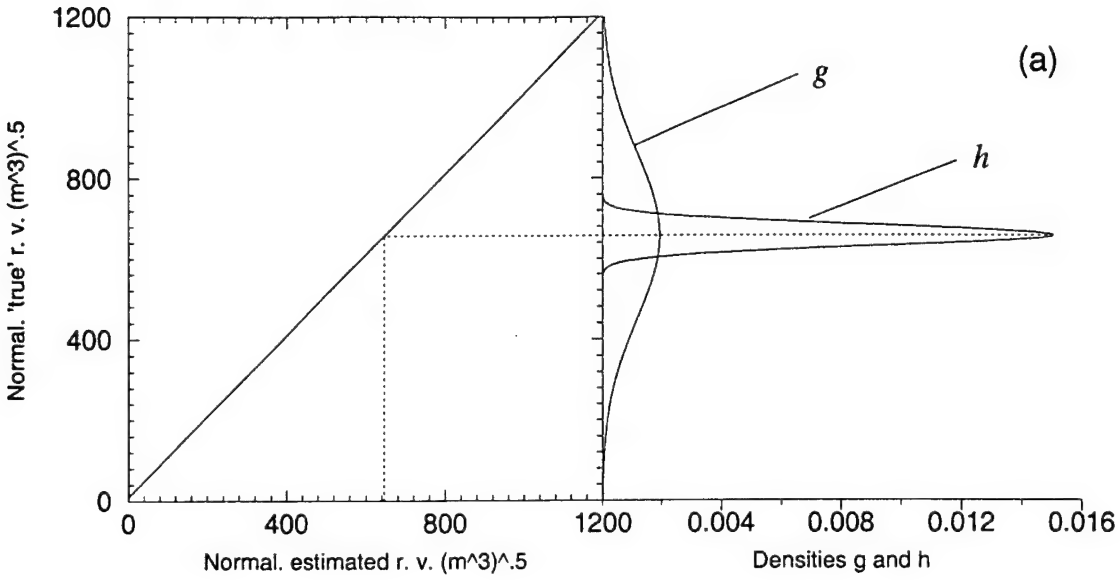
1200
800
400
0
Normal. 'true' r. v. (m^3)^.5
0
400
800
1200
Normal. estimated r. v. (m^3)^.5
g
h
(a)
0.004
0.008
0.012
0.016
Densities g and h

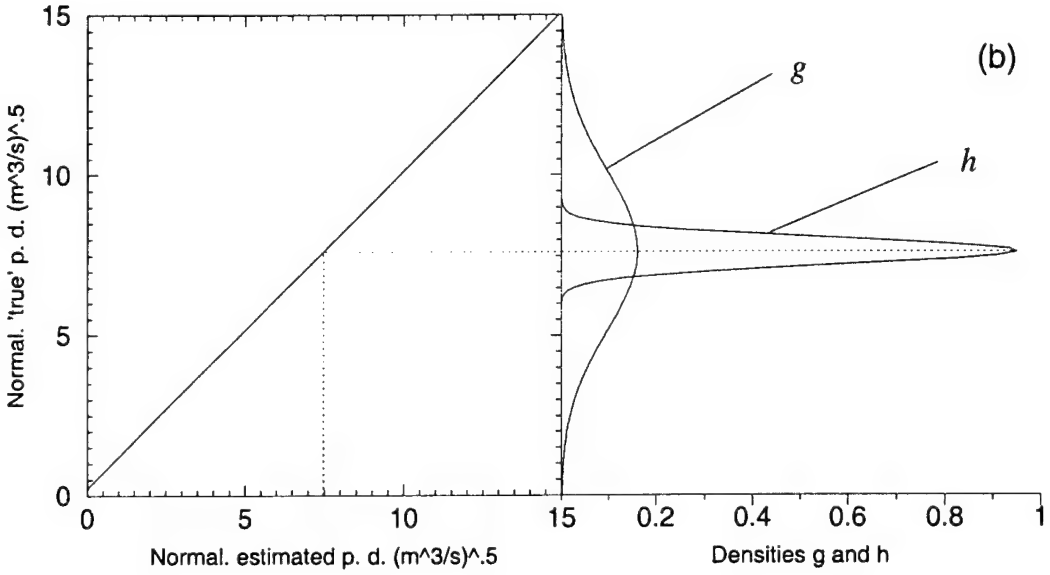
15
10
5
0
Normal. 'true' p. d. (m^3/s)^.5
0
5
10
15
Normal. estimated p. d. (m^3/s)^.5
g
h
(b)
0.2
0.4
0.6
0.8
1
Densities g and h

Figure 10

4 CONCLUSION AND RECPMMENDATIONS

A physically-based simulation framework for studying the hydrological impacts of radar-rainfall estimation errors was developed in this research. The simulation framework consists of an atmospheric model, a simulator of radar observations, and a distributed hydrologic model. The simulation framework presented in this research provides a useful tool for studying the problems of the hydrologic applications of weather radar data. In particular, the research focuses on the issue of radar-rainfall estimation uncertainty and the propagation of the errors through rainfall-runoff models.

The study demonstrates the utility of the simulation approach and considers the insight it provides. For example, it highlights the non-negligible effects of radar position (orientation) with respect to the basin, and it was able to isolate the quantitative effects of various radar-related sources of uncertainty. Results indicate that the geometry of the radar beam and coordinate transformations, due to radar-watershed-storm orientation, have an effect on radar-rainfall estimation and runoff prediction errors. In addition to uncertainty in the radar reflectivity vs. rainfall intensity relationship, there are significant range-dependent and orientation-related radar-rainfall estimation errors that should be quantified in terms of their impact on runoff predictions.

Hydrologic simulations demonstrate that radar range and orientation errors are typically amplified through predicted Hortonian runoff. In many cases, errors in runoff are

nearly twice the magnitude of rainfall volume errors. Amplification of errors is larger at locations of small total rainfall volume.

The methodology provides a tool to perform experiments to address some operational issues related to the process of radar-rainfall estimation and adjustment. Rigorous statistical analysis of the relationship between estimated rainfall errors and characteristics of the predicted hydrograph is conducted for thousands of simulated events. In addition to the influence of radar estimation error, the relationship between event magnitude and the prediction error and its propagation was analyzed. Furthermore, Application of Bayes Theorem makes it possible to quantify the uncertainty of the 'true' hydrologic variable, based on radar-estimated data, in terms of a probability distribution, conditional on all available data and knowledge and expertise of the modeler. The approach can be applied to quality-controlled radar data from different storms at a certain watershed.

The methodology developed in this research can be used to address many issues of the radar-rainfall estimation to problem that has not been addressed in this study. This study only considers convective storms and neglects the effect of bright band. Some issues of radar data quality control were not addressed (such as anomalous echo detection and elimination). Only single parameter S-band radars were considered. The significant level of some of these effects clearly indicates the need for more research on these issues. Such studies should include both simulation methods, such as the one described in this study, as well as real data-based studies.

Hopefully, through collaboration between the relevant federal agencies and the research community, it will be possible to design and conduct appropriate field and data experiments. Certainly, such experiments will ultimately lead to the improved predictive capabilities of hydrologic processes.

The methodology can be extended to perform more rigorous radar data error studies. For example, this study addressed rainfall and runoff errors at the watershed scale, but choosing a finer spatial scale might be more appropriate in many situations, especially for watersheds of larger sizes. The uncertainty associated with the modeling tools can also be integrated in the total uncertainty, which was not included in this study. These types of studies will help in understanding the uncertainty of hydrologic applications of weather radar and will prove to be very useful in making operational decisions based on radar products.

BIBLIOGRAPHY

Alonso, C. V., Hydrologic research on the USDA Goodwin Creek Experimental Watershed, northern Mississippi, *Proceedings of the 16th Annual AGU Hydrology Days Conference*, pp. 25-36, Hydrology Days Publ., Atherton, Calif., 1996.

Anagnostou, E. N., C. A. Morales, TRMM precipitation radar helps address problems of ground-based weather radar systems, *EOS*, 81(44), 2000.

Anagnostou E. N., C. A. Morales, T. Dinku, The use of TRMM precipitation radar observations in determining ground radar calibration biases, *J. Atmos. Oceanic Technol.*, 18(4), 616-628, 2001.

Anagnostou, E. N., and W. F. Krajewski, Simulation of radar reflectivity fields: Algorithm formulation and evaluation, *Water Resour. Res.*, 33(6), 1419-1429, 1997.

Austin, P. M., Relation between radar reflectivity and surface rainfall, *Month. Weath. Rev.*, 1987.

Barge, B. L., R. G. Humphries, S. J. Mah and W. K. Kuhnke, Rainfall measurements by weather radars: applications to hydrology, *Weather Resour. Res.*, 15(6), 1380-1386,

1979.

Bastidas, L. A., H. V. Gupta, and S. Sorooshian, Multi objective generalized sensitivity analysis (MOGSA) for land surface parameterization schemes, presented AGU Fall Meeting, San Francisco, CA, Fall 1997.

Battan L. J., *Radar observations of the atmosphere*, University of Chicago Press, 1973

Becchi, I., E. Caporali, and E. Palmisano, Hydrologic response to radar rainfall maps through a distributed model, *Nat. Hazards*, 9, 95-108, 1994.

Beck, M. B., Water quality modeling: A review of the analysis of uncertainty, *Water Resour. Res.*, 23(8), 1393-1442, 1987.

Beven, K. J., and A. M. Binley, The future of distributed models: Model calibration and uncertainty prediction, *Hydrol. Processes*, 6, 29-44, 1992.

Bingner, R. L., Runoff simulated from Goodwin Creek watershed using SWAT, *Trans. ASAE*, 39, 85-90, 1996.

Borga, M., E. N. Anagnostou, and W. F. Krajewski, A simulation approach for validation of

a bright band correction method, *J. Appl. Meteorol.*, 36, 1507-1518, 1997.

Brazil, L. E., "Multilevel calibration strategy for complex hydrologic models", Ph. D. dissertation, Colorado State University, Fort Collins, CO, 192 pp., 1988.

Calheiros, R. V., Local effects on climatological Z_h-R relationships, *22nd Conference on Radar Meteorology*, Am. Meteorol. Soc., Zurich, Switzerland, 341-345, 1984.

Chandrasekar, V., V. N. Bringi, N. Balakrishnan, and D. S.Zrnic, Error structure of multiparameter radar and surface measurement of rainfall, III, Specific differential phase, *J. Atmos. Oceanic Technol.*, 7, 621-629, 1990.

Chandrasekar, V., and V. N. Bringi, Error structure of multiparameter radar and surface measurement of rainfall, I, Differential reflectivity, *J. Atmos. Oceanic Technol.*,5, 783-795, 1988a.

Chandrasekar, V., and V. N. Bringi, Error structure of multiparameter radar and surface measurement of rainfall, II, X-band attenuation, *J. Atmos. Oceanic Technol.*, 5, 796-802, 1988b.

Chandrasekar, V., and V. N. Bringi, Simulation of radar reflectivity and surface

measurements of rainfall, *J. Atmos. Oceanic Technol.*, 4, 464-478, 1987.

Collier, C. G., Accuracy of rainfall estimates by radar, I, Calibration by telemetering rain gauges, *J. Hydrol.*, 83, 207-223, 1986a.

Collier, C. G., Accuracy of rainfall estimates by radar, II, Comparison with rain gauge network, *J. Hydrol.*, 83, 225-235, 1986b.

Collier, C. G., and J. M. Knowles, Accuracy of rainfall estimates by radar, III, Application for short-term flood forecasting, *J. Hydrol.*, 83, 237-249, 1986.

Crum, T. D., and R. L. Alberty, The WSR-88D and WSR-88D operational support facility, *Bull. Of the Amer. Meter. Soc.*, 74(9), 1669-1687, 1993.

Doviak, R. J., and D. S. Zrnic, *Doppler Radar and Weather Observations*, Academic Press Inc., San Diego, California, 1993.

DeGroot, M. H, *Optimal Statistical Decisions*, Chapter 9, McGraw-Hill, New York, 1970.

Droegemeier, K. K., J. D. Smith, S. Businger, C. Doswell III, J. Doyle, C. Duffy, E. Foufoula-Georgiou, T. Graziano, L. D. James, V. Krajewski, M. Lemone, D.

Lettenmaier, C. Mass, R. Pielke Sr., P. Ray, S. Rutledge, J. Schaacke, and E. Zipser, Hydrological aspect of weather prediction and flood warnings: Report of the ninth prospectus development team of the U.S. Weather Research Program, *Bull. of the Amer. Meteor. Soc.*, 81(11), 2665-2680, 2000.

Droegemeier, K. K., M. Xue, K. Brewster, Y. Liu, S. Park, F. Carr, J. Mewes, J. Zong, A. Sathye, G. Bassett, M. Zou, R. Carpenter, D. McCarthy, D. Andra, P. Janish, R. Graham, S. Sanielvici, J. Brown, B. Loftis, and K. McLain, The 1996 CAPS spring operational forecasting period: Realtime storm-scale NWP, Part I: Goals and methodology. *Preprint, 11th Conf. on Num. Wea. Pred.*, Amer. Meteor. Soc., Norfold, VA, 294-296, 1996.

Flach, J. D., T. R. E. Chidley, and A. Siyyid, New possibilities for precipitation estimation for river basin managers in developing countries, Hydrological Applications of Weather Radar, I. D. Cluckie and C. G. Collier (Editors), Ellis Horwood, 567-571, 1991.

Freer, J., K. J. Beven, and B. Ambroise, Bayesian estimation of uncertainty in runoff prediction and the value of data: An application of the GLUE approach, *Water Resour. Res.*, 32(7), 2161-2173, 1996.

Fulton, R. A., J. P. Breidenbach, D.-J. Seo, and D. A. Miller, WSR-88D rainfall algorithm, *Wea. Forecasting*, 13, 377-395, 1998.

Gao, J., M. Xue, Z. Wang, and K. K. Droegemeier, The initial condition and explicit prediction of convection using ARPS adjoint and other retrievals methods with WSR-88D data. *12th Conf. Num. Wea. Prediction*. Amer. Meteor. Soc., Phoenix AZ, 176-178, 1998.

Georgakakos, K. P., A generalized stochastic hydrometeorological model for flood and flash flood forecasting, 1, Formulation, *Water Resour. Res.*, 22(13), 2083-2095, 1986a.

Georgakakos, K. P., A generalized stochastic hydrometeorological model for flood and flash flood forecasting, 2, Case studies, *Water Resour. Res.*, 22(13), 2096-2106, 1986b.

Grecu, M. and W.F. Krajewski, Rainfall forecasting using variational assimilation of radar data in numerical cloud models, *Advances in Water Resources*, 24(2), 213-224, 2000.

Green, W. H., and G. A. Ampt, Studies on soil physics, 1. Flow of air and water through soils, *J. Agric. Sci.*, 4, 1-24, 1911.

Horton, R.E., The role of infiltration in the hydrologic cycle, *Eos Trans. AGU*, 14, 446-460,

1933.

Hudlow, M. D., D. R. Greene, P. R. Ahnert, W. F. Krajewski, T. R. Sivaramakrishnan, E. R. Johnson, and M. R. Dias, Proposed off-site precipitation processing system for NEXRAD, *Preprints of the 21st Radar Meteorology Conference*, AMS. Boston, MA, 1983.

Hunter, S., WSR-88D radar rainfall estimation: capabilities, limitations and potential improvements. *NWA Digest*, 20 (4), 26-36, 1996.

Joss, J., and A. Waldvogel, Precipitation measurement and hydrology, in: Atlas, D. (Editor), *Radar in Meteorology: Battan Memorial and 40th Anniversary Radar Meteorology Conference*, American Meteorological Society, Boston, MA, 1990.

Julien, P. Y. and G. E. Moglen, Similarity and length scale for spatially varied overland flow, *Water Resour. Res.*, 26(8), 1819-1832, 1990.

Julien, P. Y., B. Saghafian, and F. L. Ogden, Raster-based hydrologic modeling of spatially-varied surface runoff, *Water Resources Bulletin*, 31(3), 523-535, 1995.

Keesman, K. J., Set-theoretic parameter estimation using random scanning and principal

component analysis, *Mathematical Computation and Simulation*, 1990.

Kessler, E., On the distribution and continuity of water substance in atmospheric circulation. *Meteorological Monographs*, 10, American Meteorological Society, Boston, MA, 1969.

Klemp, J. B., and R. Rotunno, A study of the tornadic region within a supercell thunderstorm, *J. Atmos. Sci.*, 40, 359-377, 1983.

Klemp, J. B., R. B. Wilhelmson, and P. S. Ray, Observed and numerically simulated structure of a mature supercell thunderstorm, *J. Atmos. Sci.*, 38, 1558-1580, 1981.

Klepper, O., H. Scholten, and J. P. G. Van de Kamer, Prediction uncertainty in an ecological model of the Oosterschelde Estuary, Journal of Forecasting, 10, 191-209, 1991.

Kouwen, N., and G. Garland, Resolution considerations in using radar rainfall data for flood forecasting, *Can. J. Civ. Eng.*, 16, 279-289, 1989.

Krajewski, W. F., R. Raghavan, and V. Chandrasekar, Physically based simulation of radar rainfall data using a space time rainfall model, *J. Appl. Meteorol.*, 32(2), 268-283, 1993.

Krajewski, W.F., and J. A. Smith, On the estimation of climatological Z-R relationships, *J. Appl. Meteorol.*, 30(10), 1436-1445, 1991.

Krajewski, W.F., Cokriging of radar rainfall and rain-gauge data, *J. Geophys. Res.*, 92, 9571-9580, 1987.

Krajewski, W. F., and K. P. Georgakakos, Synthesis of radar-rainfall data, *Water Resour. Res.*, 21(5), 764-768, 1985.

Krzysztofowicz, R., Bayesian theory forecasting of probabilistic forecasting via deterministic hydrologic model, *Water Resour. Res.*, 35(9), 2739-2750, 1999.

Krzysztofowicz, R., A theory of flood warning systems, *Water Resour. Res.*, 29(12), 3981-3994, 1993.

Lin, Y., P. S. Ray, and K. W. Johnson, Initialization of a modeled convective storm using Doppler radar-derived fields, *Mon. Wea. Rev.*, 121, 2757-2775, 1993.

Mimikou, M. A., and E. A. Baltas, Flood forecasting based on radar rainfall measurements, *J. Water Resour. Plann. Manag.*, 122(3), 151-156, 1996.

Ogden, F. L., and H. O. Sharif (2000) Rainfall Input for Distributed Hydrologic Modeling-The Case for Radar, in *Proceedings of ASCE Watershed Management Conference*, Fort Collins, Colorado, June 2000.

Ogden, F. L., CASC2D *Version 1.18 Users's Manual*, Department of Civil and Environmental Engineering U-37, University of Connecticut, Storrs, CT, 06268, 1998.

Ogden F. L., and S. U. S. Senarath, Continuous distributed-parameter hydrologic modeling with CASC2D, in *Proc. XXVII IAHR Cong.*, 864-869, Int. Assoc. For Hydraulic Res., Delft, Netherlands, 1997a.

Ogden, F. L., and B. Saghafian, Green and Ampt infiltration with redistribution, *J. Irrig. Drain. Engrg.*, 123(5), 386-393, 1997b.

Ogden, F. L., and P. Y. Julien, Runoff model sensitivity to radar rainfall resolution, *J. Hydrol.*, 158, 1-18, 1994.

Pessoa, M. L., R. L. Bras, and E. R. Williams, Use of weather radar for flood forecasting in the Sieve River basin: A sensitivity analysis, *J. Appl. Meteorol.*, 32(3), 462-475, 1993.

Ray, P. S., B. Johnson, K. W. Johnson, J. S. Bradberry, J. J. Stephens, K. K. Wagner, R. B. Wilhelmson, and J. B. Klemp, The morphology of severe tornadic storms on 20 may 1977, *J. Atmos. Sci.*, 38, 1643-1663, 1981.

Salas, J. D., R. A. Smith, G. Q. Tabios III, and J-H Heo, *Statistical Computer Techniques in Hydrology and Water Resources*, Dept. of Civil Eng., Colorado State University, 1993.

Schell, G. S., C. A. Madramootoo, G. L. Austin, and R. S. Broughton, Use of radar measured rainfall for hydrologic modeling, *Can. Agric. Eng.*, 34(1), 41-48, 1992.

Senarath, S. U. S., F. L. Ogden, C. W. Downer, and H. O. Sharif, On the Calibration and verification of distributed, physically-Based, continuous, Hortonian hydrologic models, *Water Resour. Res.*, 36(6), 1495-1510.

Seo, D.-J., Real-time estimation of rainfall fields using radar rainfall and raingage data, *J. Hydrol.*, 208, 37-52, 1998.

Shah, S. M. S., P. E. O'Connell, and J. R. M. Hosking, Modeling the effects of spatial variability in rainfall on catchment response, 2, experiments with distributed and

lumped models, *J. Hydrol.*, 175, 89-111, 1996.

Shapiro, A., L. Zhao, S. Weygandt, K. Brewster, S. Lazarus, and K. K. Droegemeier, Initial forecast fields from single-Doppler wind retrieval, thermodynamic retrieval and ADAS. *Preprints, 11th Conference on Numerical Weather Prediction.* Amer. Meteor. Soc., Norfolk, VA, 119-121, 1996.

Sharif, H. O., F. L. Ogden, W. F. Krajewski, and M. Xue, Numerical Studies of Radar-rainfall Error Propagation, submitted to *Water Resour. Res.*, March 2001.

Skamarock, W. C., M. L. Weisman and J. B. Klemp, Three-dimensional evolution of simulated long-lived squall lines, *J. Atmos. Sci.*, 51, 2563-2584, 1994.

Smith, J. A., D. J. Seo, M. L. Baeck, and M. D. Hudlow, An intercomparison study of NEXRAD precipitation estimates, *Water Resour. Res.*, 32(7), 2035-2045, 1996.

Smith, J. A., and W. F. Krajewski, A modeling study of rainfall rate-reflectivity relationships, *Water Resour. Res.*, 29(8), 2505-2514, 1993.

Smith, J. A., G. N. Day, and M. D. Kane, A statistical framework for long term streamflow forecasting, *J. of Water Resour. Plann. and Manag.*, 82-93, 1992.

Spear, R. C., and G. M. Hornberger, Eutrophication in Peel Inlet, II, Identification of critical uncertainties via generalized sensitivity analysis, *Water Research*, 14, 43-49, 1980.

Steiner, M. and J. A. Smith, Reflectivity rain rate and kinetic energy flux relationships based on raindrop spectra, *J. Appl. Meteorol.*, in press, 2000.

Sun, J., and N. A. Crook, Dynamical and microphysical retrieval from Doppler radar observations using a cloud model and its adjoint, Part II: Retrieval experiments of an observed Florida convective storm, *J. Atmos. Sci.*, 55, 835-852, 1998.

Sun, J., and N. A. Crook, Dynamical and microphysical retrieval from Doppler radar observations using a cloud model and its adjoint. Part I: Model development and simulated data experiments, *J. Atmos. Sci.*, 54, 1642-1661, 1997.

Sun, J., W. Flicker, and D. K. Lilly, Recovery of three-dimensional wind and temperature fields from simulated single-Doppler data, *J. Atmos. Sci.*, 48, 876-890., 1991.

Szoke, E. J., E. J. Zipser, and D. P. Jorgensen, A radar study of convective cells in mesoscale

systems in GATE, Part I: Vertical profile statistics and comparison with hurricanes, *J. Atmos. Sci.*, 43(2), 132-197, 1986a.

Szoke, E. J., E. J. Zipser, and D. P. Jorgensen, A radar study of convective cells in mesoscale systems in GATE, Part II: Life cycles of convective cells, *J. Atmos. Sci.*, 43(2), 199-218, 1986b.

van Straten, G., and K. J. Keesman, Uncertainty propagation and speculation in projective forecasts of environmental change: A lake eutrophication example, *Journal of Forecasting*, 10, 163-190, 1991.

Vignal, B. and W.F. Krajewski, Large sample evaluation of two methods to correct range-dependent error for WSR-88D rainfall estimates, *Journal of Hydrometeorology*, 2000 (in press).

Waldvogel, A. N., The N_0 jump of raindrop spectra, *J. Atmos. Sci.*, 31, 1067-1078, 1974.

Wilson, J. W., and E. A. Brandes, Radar measurement of rainfall- a summary, *Bull. Am. Meteorol. Soc.*, 60(9), 1048-1058, 1979.

Winchell, M., H. V. Gupta, and S. Sorooshian, On the simulation of infiltration- and

saturation-excess runoff using radar-based rainfall estimates: Effects of algorithm uncertainty and pixel aggregation, *Water Resour. Res.*, 34(10), 2655-2670, 1998.

Winchell, M., H. V. Gupta, and S. Sorooshian, Effects of radar estimated precipitation uncertainty of different runoff generation mechanisms, *Tech. Rep. HWR 97-080*, 285 pp., Dept. of Hydrol. and Water Resour., Univ. Of Ariz., Tucson, 1997.

Wyss, J., E. R. Williams, and R. L. Bras, Hydrologic modeling of New England basins using radar rainfall data, *J. Geophys. Res.*, 95(D3), 2143-2152, 1990.

Xue, M., K. K. Droegemeier, V. Wong, A. Shapiro, K. Brewster, F. Carr, D. Weber, Y. Liu, and D.-H. Wang, The Advanced Regional Prediction System (ARPS) - A multiscale nonhydrostatic atmospheric simulation and prediction tool. Part II: Model physics and applications, *Meteor. Atmos. Physics*, 76, 143-165, 2001a.

Xue, M., D.-H. Wang, J.-D. Gao, K. Brewster, and K. K. Droegemeier, The Advanced Regional Prediction System (ARPS), storm-scale numerical weather prediction and data assimilation, *Meteor. Atmos. Physics*, Submitted, 2001b.

Xue, M., K. K. Droegemeier, and V. Wong, The Advanced Regional Prediction System (ARPS) - A multiscale nonhydrostatic atmospheric simulation and prediction tool.

Part I: Model dynamics and verification, *Meteor. Atmos. Physics*, 75, 161-193, 2000.

Xue, M., K. Brewster, K. K. Droegemeier, F. Carr, V. Wong, Y. Liu, A. Sathye, G. Bassett, P. Janish, J. Levit, and P. Bothwell, 1996a: Real-time numerical prediction of storm-scale weather during VORTEX-95. Part II: Operation summary and example cases, *Preprints, 18th Conference on Severe Local Storms*, Amer. Meteor. Soc., San Francisco, CA., 178-182, 1996a.

Xue, M., K. Brewster, K. K. Droegemeier, V. Wong, D. H. Wang, F. Carr, A. Shapiro, L. M. Zhao, S. Weygandt, D. Andra, and P. Janish, The 1996 CAPS spring operational forecasting period: Realtime storm-scale NWP, Part II: Operational summary and examples. *Preprints, 11th Conference on Numerical Weather Prediction*. Amer. Meteor. Soc., Norfolk, VA, 297-300, 1996b.

Xue, M., K.K. Droegemeier, V. Wong, A. Shapiro and K. Brewster, *ARPS Version 4.0 User's Guide*. Available from Center for Analysis and Prediction of Storms, University of Oklahoma, Norman OK 73072. 380 pp, 1995.

Zawadzki, I., Factors affecting the precision of radar measurement of rainfall, *22nd Conference on Radar Meteorology*, Am. Meteorol. Soc., Zurich, Switzerland, 251-256, 1984.

Zawadzki, I., The quantitative interpretation of weather radar measurement, *Atmos. Ocean*, 20,158-180, 1982.

APPNDIX I

DEVELOPMENT OF CONDITIONAL DENSITIES

The relation between the random variables E and T is modeled by building a conditional density function f(e|t). The conditional density can be built by obtaining a relation between the 'true' hydrologic variable t and the corresponding radar estimate e. Assuming a linear relation:

$$e = at + b + \varepsilon \tag{1}$$

Where a and b are constants and ε is a normal noise with 0 mean and σ^2 variance. For a given value of t, we can apply the probability rules [*Salas et al., 1993*] that:

$$\begin{aligned} E[\phi(x)] &= \phi(E[x]) \\ Var[\phi(x)] &= \left[\frac{\partial\phi}{\partial x}\right]^2 Var[x] \end{aligned} \tag{2}$$

In this case, since a, b, t are all constants, the noise ε will be the only variable in $\phi(\varepsilon)$ in (2), where $\phi(\varepsilon) = e = at + b + \varepsilon$. So, the conditional density f(e|t) will have parameters:

$$\begin{aligned} E[E \mid T = t] &= at + b \\ Var[E \mid T = t] &= \sigma^2 \end{aligned} \tag{3}$$

Now let us assume that the prior density of T, g, is normal, with or without transformation, with a mean value of μ and a variance of V^2 i.e.

$$\begin{aligned} E[T] &= \mu \\ Var[T] &= V^2 \end{aligned} \tag{4}$$

From Equations 3 and 4, the density of E can be obtained from the total probability law:

$$k(e)=\int_{-\infty}^{\infty} f(e \mid t)g(t)dt \tag{5}$$

Applying the theory of conjugate families of distributions (DeGroot, 1970), the parameters of $k(e)$ will be:

$$\begin{aligned} E[E] &= a\mu + b \\ Var[E] &= aV^2 + \sigma^2 \end{aligned} \tag{6}$$

Under conditions of normality and linearity and using Bayes Theorem, the conditional density of T, for a given value of E, will be h, where:

$$h(t \mid e)=\frac{f(e \mid t)g(t)}{k(x)} \tag{7}$$

Applying the theory of conjugate families of distributions (DeGroot, 1970), the parameters of h will be:

$$\begin{aligned} E[T \mid E = e] &= \alpha e + \beta \\ Var[T \mid E = e] &= \Pi^2 \end{aligned} \tag{8}$$

Where

$$\begin{aligned} \alpha &= \frac{aV^2}{a^2V^2 + \sigma^2} \\ \beta &= \frac{\mu\sigma^2 - abV^2}{a^2V^2 + \sigma^2} \\ \Pi^2 &= \frac{\sigma^2V^2}{a^2V^2 + \sigma^2} \end{aligned} \tag{9}$$

APPENDIX II

SIMULATION OF THE RADAR SAMPLING VOLUME

The radar sampling volume is simulated by a numbers of points within the geometric boundaries of that volume. At the location of each of these points the atmospheric variables values are read from the output of the atmospheric model. The necessary computations are then carried to compute the power returned to the radar and the radar coordinates are converted to Cartesian coordinates to prepare the input file for the hydrologic model. The following variables are defined:

phmin: minimum azimuth angle (deg.)

phmax: maximum azimuth angle (deg.)

nQo: azimuthal discretization of the resolution volume along a diagonal

nd: number of equi-spaced diagonals within the solid angle

Rj: range discretization of the resolution volume

A pseudocode of the radar of the radar beam simulation is given below:

For each of the azimuth angles considered (1 degree)

(The minimum and maximum azimuth angles are computed in a separate subroutine depending on radar orientation and distance of radar from the center of the storm domain)

do 450 iph = 1,ntheta

For each range dicretization (1km)

(The maximum range is computed in a separate subroutine depending on radar orientation and distance of radar from the center of the storm domain)

do 400 id = 1,nrange

Divide the sample volume in "Rj" range intervals

(The 1 km range is divided into 4, or more, intervals)

do 350 ir = 1,Rj

Compute the elevation of beams center

Locate nQo point along a diagonal within the sampling volume

do 200 iQ = 0,nQo

Set the number of equi-spaced diagonals

do 100 ia = 1,nd

Find Cartesian coordinates of the infinitesimal sampling volume (point)

Find the atmospheric model grid corresponding to the infinitesimal sampling volume coordinates

Compute the total attenuated reflectivity of the sampling volume

A Gaussian weight beam pattern is assumed

100 continue

200 continue

350 continue

Estimate the total reflectivity of the sampling volume

Add an N (0,1) white noise to account for the radar sampling and measurement errors

Find the corresponding (x, y) coordinates

400 continue

450 continue